Multi-Wavelength View of Kiloparsec-Scale Clumps in Star-Forming Galaxies at z∼2

Yicheng Guo[1,2], Mauro Giavalisco[1], Henry C. Ferguson[3], Paolo Cassata[1,4], Anton M. Koekemoer[3]

[1] *Astronomy Department, University of Massachusetts, 710 N. Pleasant St., Amherst, MA 01003, USA*

[2] *email: yicheng@astro.umass.edu*

[3] *Space Telescope Science Institute, 3700 San Martin Drive, Baltimore, MD, 21218, USA*

[4] *Laboratoire d'Astrophysique de Marseille, 38 avenue F. Joliot-Curie, F-13388 Marseille cedex 13, France*

ABSTRACT

This paper studies the properties of kiloparsec-scale clumps in star-forming galaxies (SFGs) at z∼2 through multi-wavelength broad band photometry. A sample of 40 clumps is identified from HST/ACS z-band images through auto-detection and visual inspection from 10 galaxies with $1.5<z<2.5$ in the Hubble Ultra Deep Field (HUDF), where deep and high-resolution HST/WFC3 and ACS images enable us to resolve structures of z∼2 galaxies down to kiloparsec (kpc) scale in the rest-frame UV and optical bands and to detect clumps toward the faint end. The physical properties of clumps are measured through fitting spatially resolved seven-band (BVizYJH) spectral energy distribution (SED) to models. On average, the clumps are blue and have similar median rest-frame UV–optical color as the diffuse components of their host galaxies, but the clumps have large scatter in their colors. Although the SFR–stellar mass relation of galaxies is dominated by the diffuse components, clumps emerge as regions with enhanced specific star formation rates (SSFRs), contributing individually ∼10% and together ∼50% of the star formation rate (SFR) of the host galaxies. However, the contributions of clumps to the rest-frame UV/optical luminosity and stellar mass are smaller, typically a few percent individually and ∼20% together. On average, clumps are younger by 0.2 dex and denser by a factor of eight than diffuse components. Clump properties have obvious radial variations in the sense that central clumps are redder, older, more extincted, denser, and less active on forming stars than outskirt clumps. Our results are broadly consistent with a widely held view that clumps are formed through gravitational instability in gas-rich turbulent disks and would eventually migrate toward galactic centers and coalesce into bulges. Roughly 40% of the galaxies in our sample contain a massive clump that could be identified as a proto-bulge, which seems qualitatively consistent with such a bulge-formation scenario.

1. Introduction

Understanding when and how the Hubble sequence observed today was formed remains an unsolved problem in astronomy. To answer it requires tracking the evolution of galaxy morphology and kinematics

back to high redshift. Thanks to the emergence of facilities with deep sensitivity and high resolution, e.g., HST/ACS, NICMOS and WFC3, galaxy morphology and structure now can be resolved into kpc scale, allowing a study on the properties of sub-structures at redshift of 2 or higher (e.g., Elmegreen & Elmegreen 2005; Elmegreen et al. 2007, 2009a,b; Gargiulo et al. 2011; Guo et al. 2011; Szomoru et al. 2011). An interesting population of galaxies at z$\sim$2, the peak of cosmic star formation activity, is star-forming galaxies (SFGs) that have star formation rate (SFR) of tens to a few hundred $\mathrm{M_{\odot}yr^{-1}}$. This population contributes a large fraction of the cosmic SFR and stellar mass density at the epoch (e.g., Daddi et al. 2007; Grazian et al. 2007; Reddy et al. 2008; Ly et al. 2011; Rodighiero et al. 2011; Guo et al. 2012). In contrast to passively-evolving galaxies at z$\sim$2, which have spheroid-like and compact morphology (e.g., Daddi et al. 2005; Trujillo et al. 2006, 2007; van Dokkum et al. 2008, 2010; Cassata et al. 2010), SFGs exhibit a wide diversity on their morphology, from smooth disk-like structure to irregular or merger-like structure (e.g., Conselice et al. 2004, 2008; Lotz et al. 2006; Ravindranath et al. 2006). A common and unique feature of SFGs at z$\sim$2 is the existence of giant kpc-scale clumps, which are associated with all types of SFGs at z$\sim$2 (e.g., Elmegreen & Elmegreen 2005; Elmegreen et al. 2007, 2009a; Bournaud et al. 2008; Genzel et al. 2008, 2011; Förster Schreiber et al. 2011) but resemble neither the starburst regions nor bulges of low redshift SFGs.

These giant clumps are mostly identified in high-resolution HST optical ACS images (e.g., Elmegreen & Elmegreen 2005; Elmegreen et al. 2007), which probe the rest-frame UV region at z$>$1 at physical spatial resolution of $\sim$1 kpc. They are also detected in HST near-infrared (NIR) images of NICMOS (Elmegreen et al. 2009a; Förster Schreiber et al. 2011), which observe the rest-frame optical wavelengths at z$>$1. Rest-frame optical line emissions from NIR integral field spectroscopy observations of z$\sim$2 disk galaxies also reveal such giant clumps (Genzel et al. 2008, 2011). Clumps are studied at even higher effective spatial resolution, up to a few $\sim$100 pc, in strongly lensed objects at 1$<$z$<$3 through rest-optical or CO line emission (e.g., Jones et al. 2010; Swinbank et al. 2010). However, the fraction of galaxies at z$\gtrsim$2 that show clumpy structures is still uncertain. Lotz et al. (2006); Ravindranath et al. (2006) and Ravindranath et al. (2011, in prep.) concluded that clumpy galaxies are only about 30% of the population at z$\sim$3, while Elmegreen et al. (2007) argued that the dominant morphology for z$\gtrsim$2 is clumpy galaxies. Wuyts et al. (2012) measured the fraction of clumpy galaxies in a mass-complete sample of SFGs at z$\sim$2 by using multi-waveband images and stellar mass maps. They found that the fraction depends sensitively on the light/mass map used to identify the clumps, decreasing from about 75% for clumps selected through rest-frame 2800 Åimages to about 40% for clumps selected through rest-frame V-band images or stellar mass maps.

The formation and subsequent evolution of these giant clumps, thought to be linked with the formation of bulges and thick disks in today's massive galaxies, are still unknown. In a widely held hypothesis based on theoretical works and numerical simulations, these kpc-scale clumps are formed through gravitational instability in gas-rich turbulent disks (e.g., Noguchi 1999; Immeli et al. 2004a,b; Elmegreen et al. 2008; Dekel et al. 2009b; Ceverino et al. 2010, 2012). This scenario is supported by the fact that high-redshift galaxies are gas-rich, with the gas–to–baryonic fraction of 20% to 80% (e.g., Erb et al. 2006; Genzel et al. 2008; Tacconi et al. 2008, 2010; Förster Schreiber et al. 2009; Daddi et al. 2010), possibly as a result of smooth and continuous accretion of cold gas flow (Kereš et al. 2005; Rauch et al. 2008; Dekel et al. 2009a;

Cresci et al. 2010; Steidel et al. 2010; Giavalisco et al. 2011). Due to the clump interactions and dynamical friction against the surrounding disks, these clumps would migrate toward the gravitational centers of their host galaxies and eventually coalesce into a young bulge as the progenitor of today's bulges or be disrupted by either tidal force or stellar feedback to form part of a thick disk (e.g., Bournaud et al. 2009; Dekel et al. 2009b; Murray et al. 2010; Genel et al. 2012).

To confirm or set constrains on the above scenarios, one needs accurate measurements on the physical properties of clumps, such as stellar mass, age, SFR, and star formation history (SFH) as well as their radial variations across the host galaxies. Such knowledge, unfortunately, is lacking and difficult to obtain, because it requires spatially resolved multi-band photometry or spatially resolved spectroscopy of each clump. In the work of Förster Schreiber et al. (2011), only two of their six galaxies have marginally enough information to enable a rough measurement on M/L and age for clumps, one with a single ACS/F814W - NIC2/F160W color and the other with Hα equivalent width measured by the adaptive optical assisted SINFONI. Their finding of evidence of a systematic trend of older clumps at smaller galactocentric radius is consistent with the above scenarios, but suffers from a small number statistics. Elmegreen et al. (2009a) studied clump clusters and chain galaxies in the HUDF with *HST*/ACS and NICMOS images. They fit stellar population models to the multi-band photometry of clumps and bulges to derive their stellar masses and ages. However, the resolution of their NICMOS images is three times poorer than that of the ACS images so that obtaining uniform multi-band photometry for individual clump is affected by the blend of clumps in the low-resolution images. Recently, Wuyts et al. (2012) performed a detailed analysis on the spatially resolved colors and stellar populations of a large and complete sample of massive SFGs at $0.5 < z < 2.5$ in the ERS and CANDELS-Deep region of GOODS-South. The multi-wavelength images of *HST*/ACS and WFC3 allow them to study light maps in both rest-frame UV and rest-frame optical with similar spatial resolutions. Their results are consistent with an inside-out disk growth scenario with a "Christmas tree" model in which giant star-forming clumps are formed through gravitational instabilities in gas-rich disks, and then are quickly disrupted through feedbacks. Alternatively, the presence of blue and young star-forming clumps superposed on a redder underlying disk in their SFGs is also consistent with the inward migration scenario. However, Wuyts et al. (2012) focused on regions with excess surface brightness and did not subtract the diffuse light of host galaxies from clumps.

In this paper, we try to measure the physical properties of clumps in SFGs at z$\sim$2 in a sufficiently large sample, exploiting the advantage of high resolution and deep sensitivity of HST/ACS and WFC3 images in the HUDF. The recently available WFC3 images allow us to measure spatially resolved multi-band photometry across the rest-frame UV and optical regions at this redshift. Especially, the WFC3 F160W image observes light with rest-frame wavelengths longer than the Balmer break, enabling an accurate measurement on the age and stellar mass of clumps. On the other hand, the high resolution of WFC3 images ($0.15''$) enables us to resolve into $\sim$1 kpc scale, a typical size of clumps, at z$\sim$2 to effectively separate the light from clumps and their surrounding disks. In this work, we compare the properties of clumps to those of their surrounding materials (Sec. 4) and also study the radial variations of clump properties across their host galaxies (Sec. 5).

Throughout the paper, we adopt a flat ΛCDM cosmology with $\Omega_m = 0.3$, $\Omega_\Lambda = 0.7$ and use the

Hubble constant in terms of $h \equiv H_0/100\mathrm{km\ s^{-1}\ Mpc^{-1}} = 0.70$. All magnitudes in the paper are in AB scale (Oke 1974) unless otherwise noted.

2. The Data and Sample Selection

2.1. Images and Catalogs

The ultra-deep ACS images in the HUDF (Beckwith et al. 2006) cover an area roughly equal to the footprint of the ACS/WFC FOV in the same four filters as the GOODS ACS program, namely F435W (B), F606W (V), F775W (i), and F850LP (z) down to a depth of 29.4, 29.8, 29.7, and 29.0 mag (5σ, $0.35''$-diameter aperture), respectively. We use the publicly available images, which have been re-binned to the same pixel scale as the GOODS/ACS mosaic, namely $0.03''$ /pixel ($0.6\times$ the original ACS pixel scale).

The WFC3/IR data are from the *HST* Cycle 17 program GO-11563 (PI: G. Illingworth), which aims at complementing the HUDF and the two HUDF05 parallel fields (Oesch et al. 2007) with WFC3/IR images in Y (F105W), J (F125W), and H (F160W) of matching sensitivity, $\sim$29 mag (Bouwens et al. 2010; Oesch et al. 2010). Here we use only the first epoch of the images, released in September 2009, which includes 18 orbits in Y, 16 orbits in J, and 28 orbits in H. We have carried out our independent reduction of the raw data, and after rejecting images affected by persistence in the J band, our final stacks reach 1σ surface brightness fluctuations of 27.2, 26.6 and 26.3 AB/$''^2$ in the three bands, respectively, over an area roughly equal to the footprint of the WFC3/IR camera ($2.1\ '' \times 2.1\ ''$). We have drizzled the WFC3 images from their original pixel size of $0.121'' \times 0.135''$ to $0.03''$ per pixel to match the scale of the GOODS and HUDF ACS images. Further details on the production of the WFC3 data are given in Koekemoer et al. (2011).

In addition to the *HST* /ACS and WFC3/IR images in the HUDF, the data used in this paper also include panchromatic multi–wavelength photometry obtained as part of the GOODS program, as the HUDF field is embedded in the GOODS south field. The long wavelength baseline of the GOODS photometry enables us to reliably select SFGs based on photometrically–derived stellar mass and specific star formation rate (SSFR), while the deep *HST* optical and NIR images allow us to obtain color maps of the galaxies with a resolution of ~ 1 kpc.

The GOODS south field has been observed with various telescopes and instrument combinations, from the X–ray to the sub–millimeter and radio. Relevant to our analysis here is the VLT/VIMOS ultra–deep U–band imaging (Nonino et al. 2009), as well as *HST*/ACS BViz (Giavalisco et al. 2004)), VLT/ISAAC JHK, Spitzer/IRAC 3.6, 4.5, 5.7, 8.0 μm, and Spitzer/MIPS 24 μm imaging. Because the resolution of the images significantly changes from optical- to IR-bands, we use an object template-fitting software dubbed TFIT (Laidler et al. 2007) to obtain matched multi–band photometry. The detailed description of TFIT measured catalog of GOODS-S can be referred from Dahlen et al. (2010); Guo et al. (2012).

2.2. Sample

In this work, we select SFGs with 1.5<z<2.5 in the HUDF to study their clumps. Since we are measuring spatially resolved properties of galaxies through photometry of only seven bands (ACS BViz and WFC3 YJH), in order to reduce the number of free SED-fitting parameters, we restrict our sample to only contain galaxies that have spectroscopic redshifts. The use of spectroscopically observed galaxies reduces a major uncertainty of SED-fitting, namely the uncertainty of (photometric) redshift. However, it also reduces the size of our sample and might bias our sample towards the bright end. In the HUDF, only 15 SFGs (SSFR $> 0.01\mathrm{Gyr}^{-1}$) have spectroscopic redshift (spec-z) at 1.5<z<2.5 to enter our sample. We visually inspect the z-band images of these galaxies and exclude five galaxies that have no obvious multi-clump morphology.

About 67% (10 out of 15 galaxies) of our sample are multi-clump systems in their optical ACS z-band (rest-frame UV) images. This result is quite similar to what Elmegreen et al. (2007) found, namely the majority of SFGs at z$\sim$2 is clumpy galaxies. It is also consistent with the clumpy fraction that Wuyts et al. (2012) measured through rest-frame UV light. However, we also note that due to the use of spec-z, our sample is small and possibly biased toward UV bright galaxies. The bright UV emission may further suggest that our sample is biased toward bluer (e.g., van Dokkum et al. 2006; Förster Schreiber et al. 2009) and more active galaxies among all SFGs at z$\sim$2. Moreover, as shown by the recent work of Wuyts et al. (2011), actively star-forming galaxies tend to have the largest sizes (see also, e.g., Franx et al. 2008), which presumably introduces a further bias in our sample toward large galaxies. To draw a robust conclusion on the fraction of clumpy galaxies at z$\sim$2, a large sample (perhaps with photometric redshift) covering a wide range of both luminosity and stellar mass is needed. The ongoing 902-orbit *HST* Multi-cycle Treasure Program, Cosmic Assembly Near-infrared Deep Extragalactic Legacy Survey (CANDELS Grogin et al. 2011; Koekemoer et al. 2011) has already begun to provide deep images over a large sky area to answer this question as well as to provide robust statistics on clump properties, as demonstrated by Wuyts et al. (2012). We also anticipate that the present paper may lay the groundwork for future studies in the CANDELS survey. The z-band, H-band, and z-H mosaics of the 10 galaxies in our sample are shown in Figure 1. The properties of the galaxies are shown in Table 1.

Three galaxies in our sample are discussed in Elmegreen & Elmegreen (2005): Galaxy 22284 (with ID 3484 in Elmegreen's paper), 21739 (Elmegreen ID 3465+), and 27101 (Elmegreen ID 6462+). These galaxies, classified as "clump-clusters" in the paper, were chosen to study by Elmegreen et al. because of their large angular size, good resolution into clump and interclump regions. Elmegreen & Elmegreen (2005) used visual inspection on ACS i-band to identify clumps. They identified more clumps in these galaxies than we find (see Table 3). Although the different selection bands may contribute, the different numbers of identified clumps in the two works could be mainly due to different clump identification strategies. We conservatively ask clumps to be 3σ brighter than the diffuse components of the host galaxies (see the next section), while Elmegreen & Elmegreen (2005) simply ask clumps to be bright compared to the sky background. We will discuss the derived properties of clumps in the two works in Sec. 6.1.

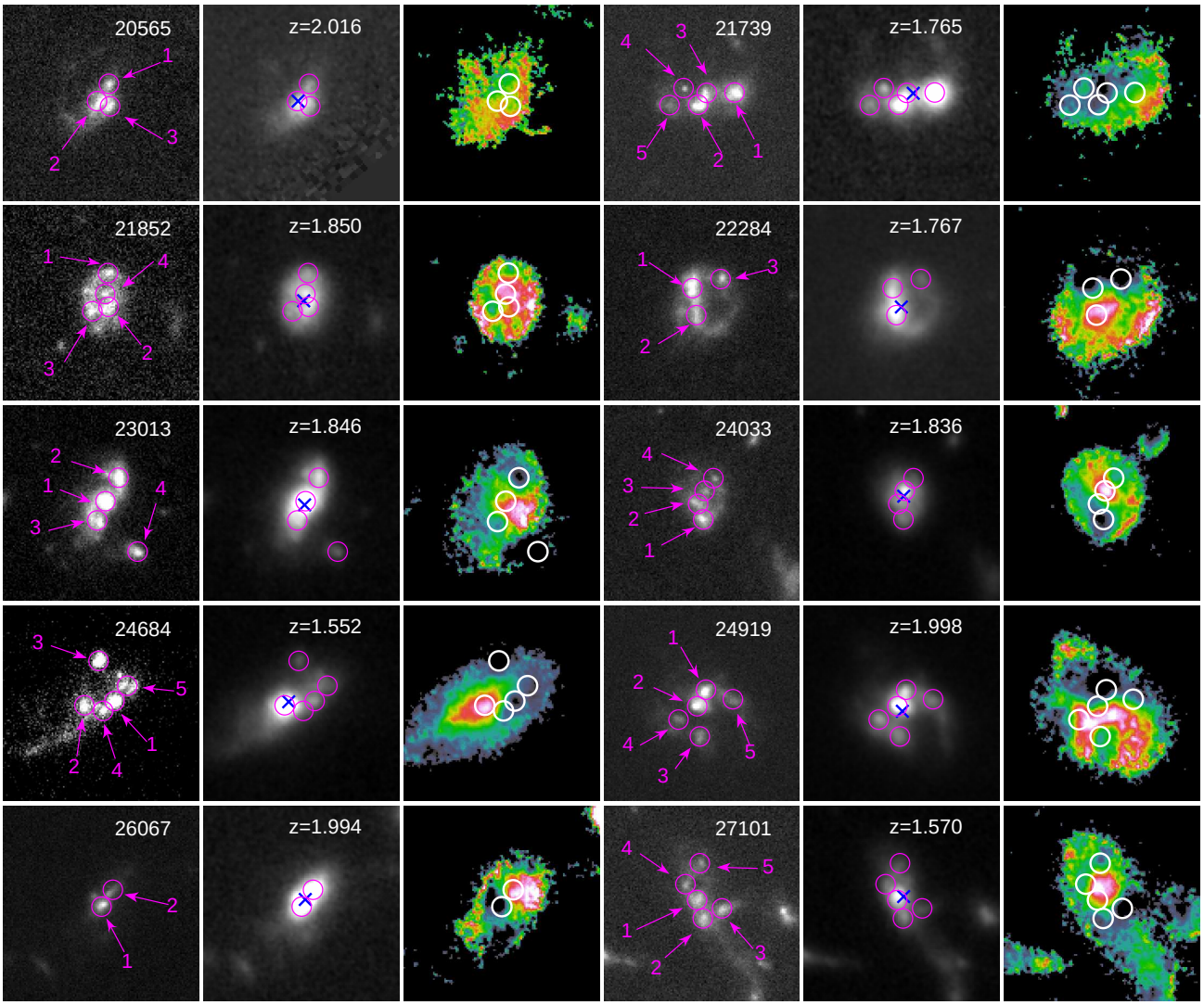

Fig. 1.— Montage of our 10 clumpy star-forming galaxies at z∼2. Each row shows images of two galaxies. For each galaxy, the panels from left to right show the z-band, H-band and z-H maps. Their galaxy IDs are shown in their z-band images, while redshifts in their H-band images. Small circles (magenta in the z-band and H-band images, and white in the z-H maps) show the identified clumps. Blue "X" in the H-band images show the light-weighted centers.

3. Clump Detection and Measurement

Clumps are detected from the HST/ACS z-band images through a hybrid of automated detection and visual inspection. In the image of each galaxy, a clump is identified if a region contains at least six contiguous pixels that are brighter than 3σ confidence level of the average surface brightness of the galaxy. If two or more sub-structures above 3σ of the average surface brightness of the galaxy are adjoining, we visually separate them and determine the peak of each clump. The locations of each identified clumps are shown by circles in the z-band images of galaxies in Figure 1.

Our choice of the ACS z-band as the detection band of clumps raises a question: how do the number and nature of identified clumps depend on the choice of the detection band? The question lies in two folds: (1) the impact of the spatial resolution of images on clump identification and (2) the impact of the use of different bands that are dominated by light of different stellar populations on clump identification. This problem was highlighted by Förster Schreiber et al. (2011), who found that, for one galaxy in their sample, clumps identified through WFC3 H-band and ACS i-band images have different physical proprieties. To test the robustness of our clump identification through the rest-frame UV band, we carry on the following two tests. First, we smooth the ACS z-band images of clumps to match the resolution of WFC H-band and repeat our identification procedure. Only one clump (#4 of 24033) is missed, and three pairs of clumps (#2 and #3 of 20565; #2 and #3 of 21739; and #1 and #2 of 26067) are blended in the smoothed images. Given the fact that only 10% (4 out of 40) of our identified clumps are affected, we conclude that the change of resolutions of images (from ACS to WFC3) would not have significant impact on our clump identification and hence our later results.

The second test is to identify clumps directly from WFC H-band images, which sample the evolved stellar populations at z$\sim$2. Besides suffering from the impact of resolution, the H-band detection misses a non-negligible fraction, $\sim$20%, of clumps that are detected in the z-band. The missed clumps are #5 of 21739; #4 of 23013; #2 and #4 of 24033; #3 and #4 of 24684; #3, #4 and #5 of 27101. These clumps are missed mainly because of lower contrast of clumps against the background diffuse stellar population in the H-band, and most of them are faint even in the z-band. Two clumps that are bright in the z-band but not detected in the H-band are #4 of 23013 and #3 of 24684. An important result in this test is that we do not find any new detected clumps through using the H-band images. This is different from the case of Förster Schreiber et al. (2011), and can be attributed to the ultra-deep rest-frame UV images used in our study, which allows us to probe even rest-frame UV faint (and hence very red) clumps. Thus, we conclude that our clump identification through ACS z-band images is superior to that through WFC H-band images, as the H-band detected clumps are just a sub-sample of the z-band detected ones. Using the z-band images, we are able to study the nature of clumps in a wide range of physical properties.

For each identified clump, we measure its multi-band photometry from ACS BViz and WFC3 YJH images, all smoothed to match the resolution of the WFC3 H-band image ($\sim$0.15″). The details and tests done to ensure an accurate PSF matching can be found in Guo et al. (2011). The fluxes of clumps in each band are measured within an aperture with size (diameter) of 0.3″, about two times the FWHM of the H-band images. In order to separate the light of clumps from that of diffuse components of galaxies, we subtract a

diffuse background from the flux of each clump. The surface brightness of the background is calculated as the average flux per pixel of the host galaxy, after all clumps in it (circles with diameter of 0.3″) are masked out. The product of the surface brightness and area of a clump is then subtracted from the flux of the clump. The diffuse background is subtracted for all clumps in all seven bands.

It is important to note that for all clumps in one galaxy, we subtract a *constant* diffuse background across the whole galaxy. This subtraction might be over-simplified, as the underling diffuse or "disk" component of a galaxy is likely to have a non-constant profile (e.g., an exponential disk profile). In that case, we would over-subtract background for clumps in outskirts of the galaxy, while under-subtract it for those close to the center. We argue that this over-simplified subtraction would not significantly change our results on the comparison of clump properties and "disk" properties, as on average, only 15% of the raw flux of each clump is subtracted. However, it may induce false signals into our studies on the radial variation of clump properties across the host galaxies. We will discuss its influence later (Sec. 5.3). We also note that the amount of subtraction is comparable to the photometric uncertainty that is caused by our use of the arbitrary d=0.3″ aperture. When we enlarge or shrink our aperture size by 2 pixels, the typical change on flux is about 15%∼20%. Therefore, we use the difference of the fluxes measured at $d \pm 0.06''$ as the uncertainty of fluxes of clumps.

The physical properties of clumps are measured through fitting seven-band SEDs to stellar population synthetic models. We use the updated version (CB09, Charlot & Bruzual in prep.) of Bruzual & Charlot (2003), which includes a new treatment on the contribution of TP-AGB stars, as our stellar population library. The initial mass function (IMF) of Salpeter (Salpeter 1955) is used. The redshifts of all clumps are fixed at the spec-zs of their host galaxies during the fitting. Since the SFH of galaxies at z∼2 is controversial (e.g., Lee et al. 2009, 2010; Maraston et al. 2010; Papovich et al. 2011), we fit each clump with three different types of SFHs: exponential declining (τ-model), constant (CSF), and exponential increasing. Among the three fits of each clump, the one with the smallest reduced χ^2 is chosen as the best-fit model and its corresponding parameters are used as the physical properties of the clump. For each fitting parameter, we use the standard deviation of the three best-fit values from different SFHs as the uncertainty of the parameter, as we believe that the largest uncertainty of SED-fitting is rooted from the uncertainty of SFHs. We fix the metallicity to the solar value for all clumps. We will discuss the influence of metallicity variation among clumps on our results later (Sec. 5.4). When deriving the physical properties from the best fit template, we adopt the following definitions. To measure SFR, we average the SFH of the best fit template over the last 100 Myr, which allows a meaningful comparison between SFR derived through SED-fitting and that through rest-frame UV continuum empirically. The age of objects in our paper corresponds to the time from the onset of their star formation to their redshifts. And our stellar mass measurement accounts for the loss of stellar mass over time.

We also measure the fluxes and properties of the diffuse component (called "disk" thereafter) in each galaxy. The flux of a "disk" is measured by subtracting the total fluxes of clumps in its host galaxy from the flux of the galaxy. The physical properties of "disks" are measured with the same method that is used for clumps. We note that whether these diffuse components are real disks or not is still unknown. Actually, it is a key to understand the formation mechanisms of clumps. The existence of underlying disks is a

necessary condition for the scenario of fragmentation due to gravitational instability. Kinematic studies, e.g., Förster Schreiber et al. (2009), are needed to understand the nature of the diffuse components. In this paper, we just call them "disks" for simplicity.

The properties of clumps and "disks" are shown in Table 2.

4. Physical Properties of Clumps

4.1. Rest-frame UV–Optical Color of Clumps

To understand the nature of our clumps, we study their positions in color–magnitude diagram (CMD). In CMD, present-day galaxies are well separated into two populations: red-sequence and blue cloud (e.g., Blanton et al. 2003; Bell et al. 2004). This color bimodality is observed to exist up to z$\sim$1.5 (e.g., Bell et al. 2004; Brammer et al. 2009; Mendez et al. 2011). The red-sequence is believed to consist of old and quiescent galaxies, while the blue cloud consists of young and active galaxies. The locations of clumps in CMD, namely among red-sequence or blue cloud, would shed a light on whether they are as quiescent as local red spheroids/bulges or still actively forming stars.

Figure 2 shows the diagram of rest-frame (U-V) color vs. absolute rest-frame V-band magnitude for clumps (starred symbols). Rest-frame magnitudes are obtained through interpolating the observed seven-band photometry to corresponding rest-frame wavelength, based on the redshift of each clump. In the figure, we also plot the "disks" (triangles) and host galaxies as a whole (circles). We also plot the six passively-evolving galaxies from Guo et al. (2011) (squares) in the figure. The separation of red-sequence and blue cloud shifts blueward as the redshift increases, because the cosmic age decreases with redshift. To obtain a red-blue separation line for z$\sim$2, we extrapolate the separation line at z=0 of Bell et al. (2004) to z=2 with the empirical evolving formula proposed in their paper: $< U-V >= 1.23-0.4z-0.08(M_V-5logh+20)$. The red–blue separation lines at z=0 and z=2 are shown by dashed and solid lines in the figure.

In general, clumps are as blue as their surrounding "disks" and host galaxies. Only few clumps reach above the red–blue sequence at z=2 and might have properties similar to quiescent galaxies at z$\sim$2. Overall, the blue color indicates that the star formation activity is still strong and has not been widely quenched in clumps. We note that our clumps are identified through the excess of the rest-frame UV light in the diffuse background. Therefore, we expect them to have *bluer* color than their surrounding "disks". However, Figure 2 does not support such expectation. What's more, it shows that, compared with "disks" or host galaxies, clumps seem to have broader color dispersion. This broader scatter suggests that our clumps cover a wide range of physical properties (e.g., age or extinction), have diverse star formation histories, or are in different evolution stages. This result seems contradictory to the simple "Christmas tree" model, in which clumps are rapidly disrupted once they have formed. In that case, the properties of clumps may concentrate within a narrow range. We will quantify the dispersion of clump colors in Sec. 4.4.

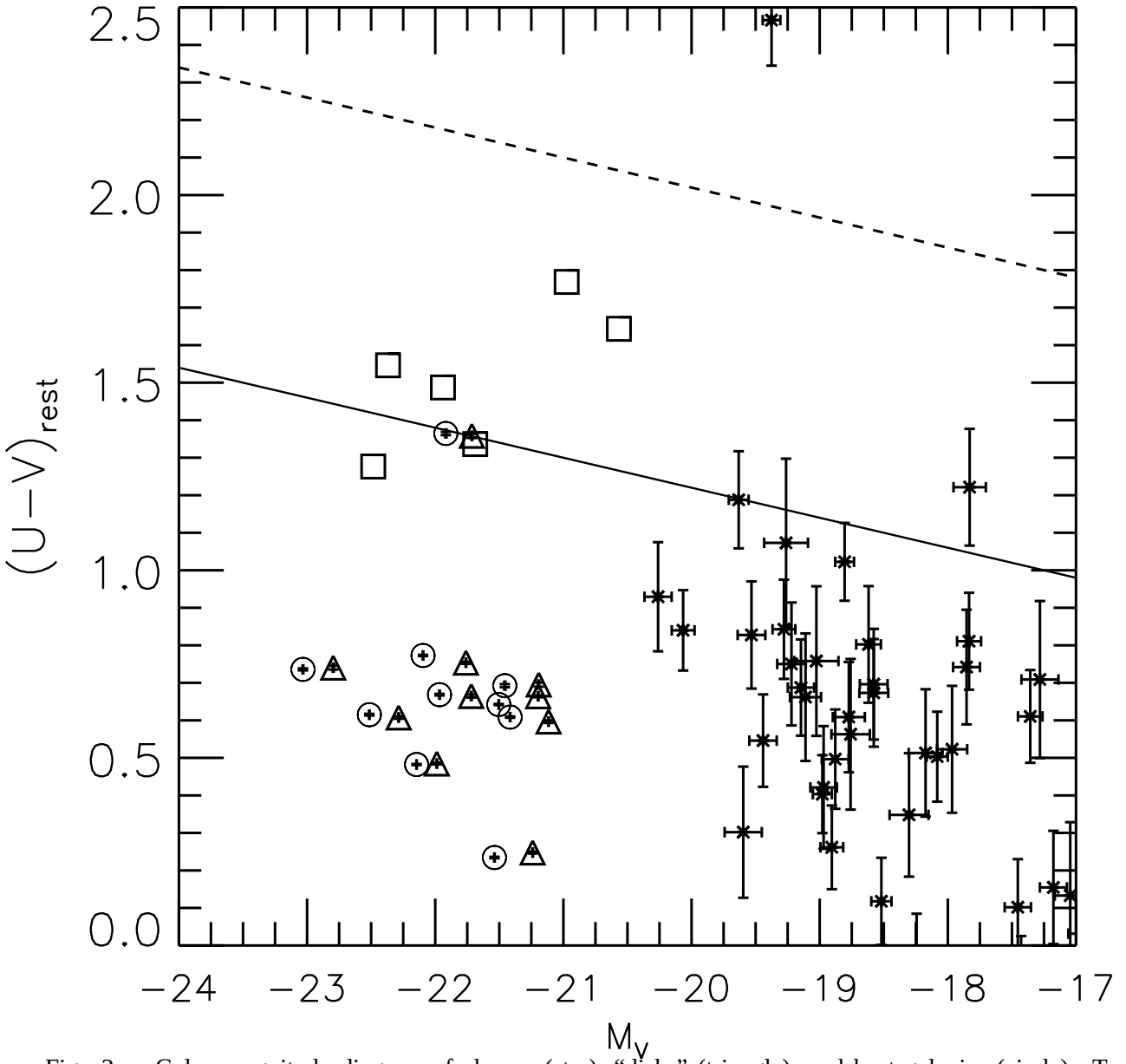

Fig. 2.— Color–magnitude diagram of clumps (star), "disks" (triangle), and host galaxies (circle). Together plotted are six passively-evolving galaxies at z∼2 (squares) from Guo et al. (2011). We also plot the separation of red-sequence and blue cloud at z=0 from Bell et al. (2004) (dashed line). The solid line is the extrapolation of the separation from z=0 to z=2 by using the formula of evolution of the separation of Bell et al. (2004).

4.2. SFR–Stellar Mass Relation of Clumps

Figure 3 shows the SFR–stellar mass relation of clumps (red stars) as well as that of "disks" (blue triangles) and whole galaxies (black circles). SFR and stellar mass are measured through SED-fitting with various assumed SFHs as described in Sec. 3. The best linear fit for the relation of each population is also shown in the plot. In order to evaluate the significance of the SFR–stellar mass relation of both clumps and "disks", we run bootstrapping 100 times to randomize the pair of SFR and stellar mass of clumps and disks and calculate the correlation coefficients (defined as $\sqrt{\mathrm{COVAR[X,Y]/(VAR[X]*VAR[Y])}}$, where COVAR is covariance and VAR is variance of X and Y, and X and Y stand for stellar mass and log(SFR)) for both the observed and randomized relations. By comparing the correlation coefficients of both the observed and randomized relations, we find the relation of both clumps and "disks" are significant at at least 3σ level. The SFR–stellar mass relation of clumps and "disks" have almost the same slope, although the two populations occupy different ends of the stellar mass range: the stellar masses of clumps spread over the range between $10^{8}\mathrm{M}_{\odot}$ and $10^{10}\mathrm{M}_{\odot}$, while those of "disks" between $10^{10}\mathrm{M}_{\odot}$ and $10^{11}\mathrm{M}_{\odot}$. However, the normalization of the relation of clumps is about five times higher than that of "disks", converting to a higher SSFR of clumps. The higher SSFR is consistent with the spectroscopic measures of Genzel et al. (2011).

The reason of the higher SSFR of clumps is important for understanding the nature of clumps, but unfortunately still unknown. It could be due to the fact that the locations of clumps sample the very high end of the gas density distribution of host galaxies. As a sequence, the gas–to–stellar mass ratio is higher in clumps than in "disks". This case is likely true, as these clumps are believed to form through gravitational instability in the gas-rich "disks". Such process indicates a high gas density in their birth locations. However, based on our later analysis, the (projected) stellar mass density of clumps is also higher than that of "disks". Therefore, it is still uncertain whether the gas–to–stellar mass ratio of clumps is comparable for that of "disks". If they are comparable, clumps would have higher efficiency to convert gas into stars to yield higher SSFR. In this case, other mechanisms, for example a different star-formation law, should be used to explain the higher star formation efficiency of clumps. Further observations on spatially resolved gas density (e.g., through ALMA) are required to investigate the star formation activity in clumps.

Figure 3 also shows that the SFR–stellar mass relation (or SSFR) of the galaxies as a whole has almost the same slope and normalization as that of "disks". It suggests that "disks" contribute the majority fraction of SFR and stellar mass of the host galaxies. Clumps, on the other side, stand out as regions with enhanced SSFR in the "disks".

4.3. Contribution of Clumps to Host Galaxies

Figure 4 shows the fractional contributions of clumps to their host galaxies, in terms of rest-frame U-band and V-band luminosity, stellar mass and SFR. We show the distribution of the contributions of both each individual clump (solid line) and the sum of all clumps in one galaxy (dashed line). For the U-band and V-band luminosity (top left and top right panels), the individual contribution of clumps runs from 1% to 10%, with a median of $\sim$5%, while the total contribution of all clumps sharply peaks around 20%. There

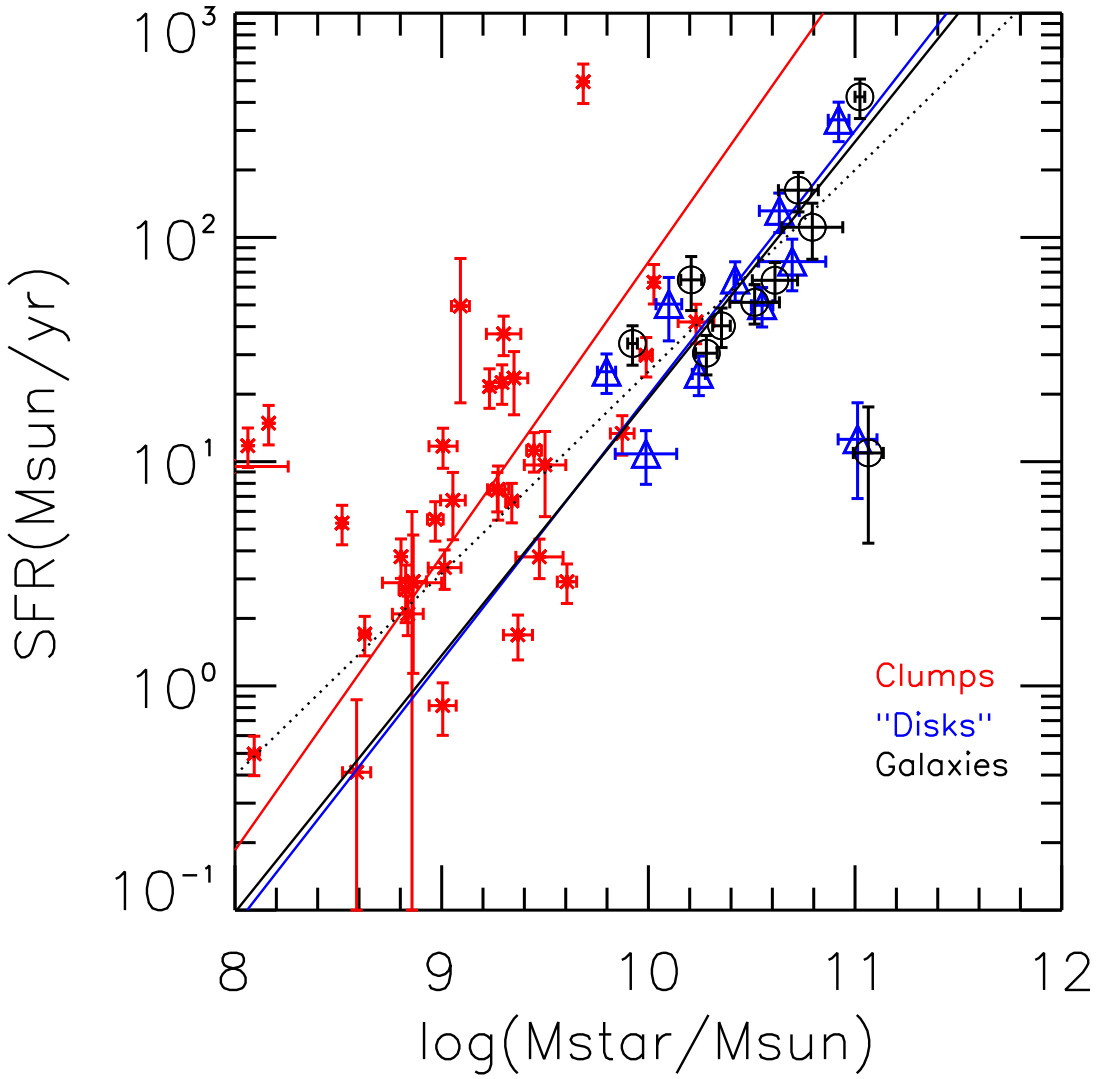

Fig. 3.— SFR–stellar mass relation for clumps (star), “disks” (triangle), and host galaxies (circle). The SFR–stellar mass relation of each population is fitted by a straight line (red, blue, and solid black for clumps, “disks”, and host galaxies, respectively). The dotted line is the relation of Daddi et al. (2007) for BzK galaxies.

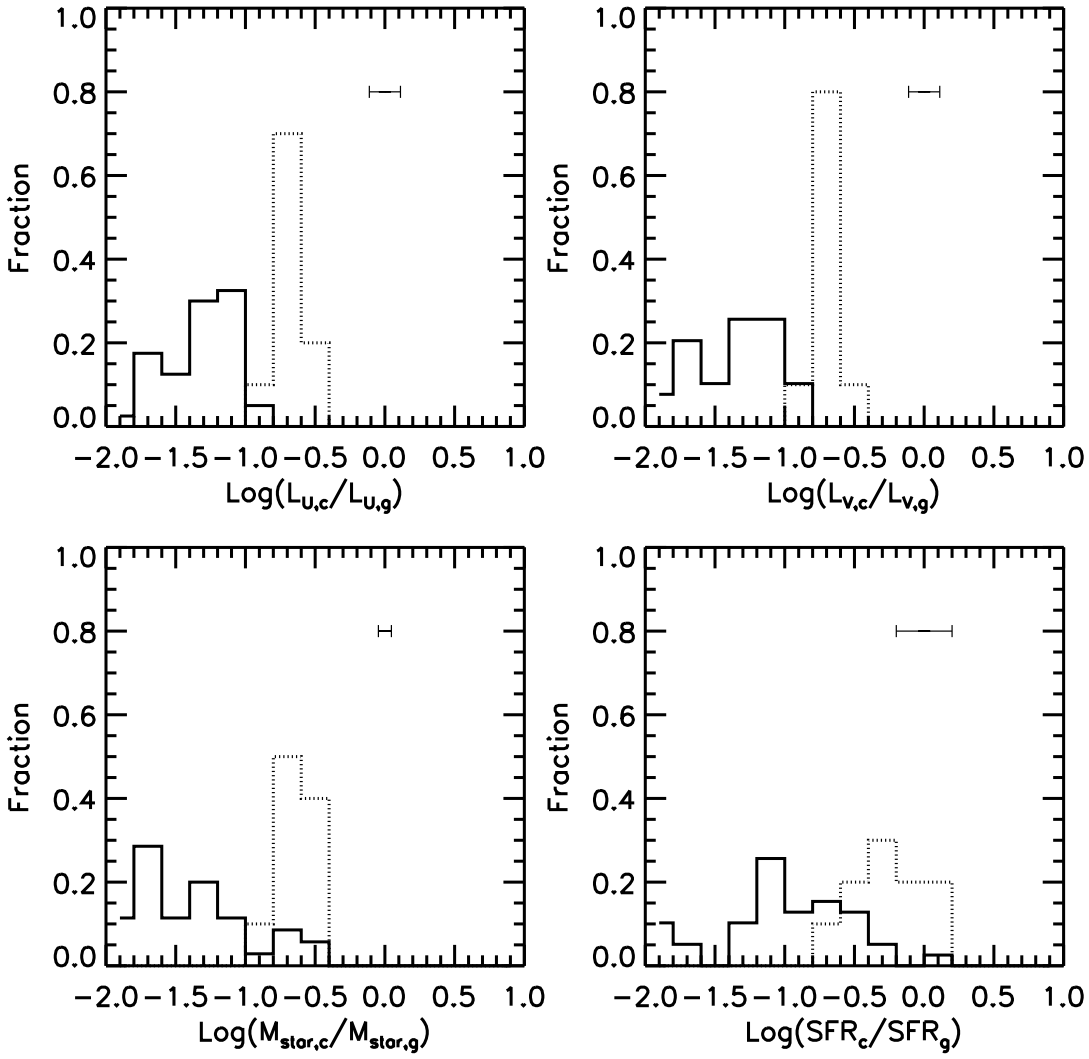

Fig. 4.— Fractional contributions of clumps to their host galaxies in terms of rest-frame U-band luminosity (top left), V-band luminosity (top right), stellar mass (bottom left), and SFR (bottom right). Solid histograms show the distributions of the contribution of each clump, while dotted lines show the distributions of the total contribution of all clumps in each host galaxy. The horizontal error bar in each panel shows the typical error of each measurement.

is no obvious difference between the clump contributions to both luminosities. The clump contribution to stellar mass (bottom left) is similar to that of the light, with a broad distribution of individual contribution running from 1% to more than 10%, and a concentrated total contribution peaking around 20%. We note that the similar contributions to stellar mass and to light of individual clumps do not imply a similar M/L ratio among clumps. Actually, the $\mathrm{M/L_V}$ ratio of clumps covers a wide range, from $\sim$0.05 $\mathrm{M_\odot/L_{\odot,V}}$ to several $\mathrm{M_\odot/L_{\odot,V}}$, with the median of 0.5 $\mathrm{M_\odot/L_{\odot,V}}$ and the standard deviation of 0.5 dex. The widespread M/L ratio of clumps is consistent with our previous argument that clumps are found at different evolutionary stages.

The contribution of clumps to SFR (bottom right) is higher than that to light and stellar mass. The individual contribution peaks around 10%, while the total contribution peaks around 50%. The low contribution to stellar mass and high contribution to SFR are consistent with the fact the clumps have enhanced SSFR relative to "disks" or galaxies as a whole.

4.4. Clumps vs. "Disks"

Figure 5 shows the difference between clumps and "disks" in terms of the distributions of UV–optical colors (top left), ages (top right), dust extinction (bottom left) and projected stellar mass densities (bottom right) of clumps (red) and "disks" (blue). Each distribution is fitted by a Gaussian function. This figure shows that the mean UV–optical color of clumps is similar to that of disks (U-V$\sim$0.6). However, the color distribution of clumps is broader than that of disks. The standard deviation of the former is 0.30, while that of the latter is 0.12. Clumps can be as red as U-V$\sim$1.2 and as blue as U-V$\sim$-0.2, while "disks" are concentrated within 0.2$<$U-V$<$0.8, except for one "disk". The broader color distribution of clumps can be attributed to either different SFHs among clumps or different evolution stages of clumps.

Our SED-fitting method only provides limited information on SFHs, however, the distribution of ages of clumps gives us a hint that the broader color distribution of clumps is more likely associated with the evolution stages. On average, the ages of clumps are only slightly (0.2 dex) younger than that of "disks". However, the ages of clumps have a broader distribution, covering the range from 0.01 Gyr to a few Gyr, with the standard deviation of 2.1 dex. In contrast, the ages of "disks" are concentrated within 0.3 to 1 Gyr, with a standard deviation of 1.7 dex. Moreover, in Sec. 5, we will show that both color and age of clumps change with the galactocentric distance of clumps. Based on the trend of their radial variations, one can expect a loose correlation between colors and ages of clumps, which would support our speculation that the broader color distribution of clumps is due to the broad age distribution (and hence different evolution stages). However, we note that the age determination in SED-fitting is not robust and strongly depends on the assumed SFHs. As shown by the horizontal error bars in the top right panel, the uncertainty of age in our study, namely the standard deviation of the ages measured by SED-fitting with three different SFHs, is about 0.5 dex and 0.3 dex for clumps and "disks" respectively, larger than the difference between the mean age of the two populations.

We also argue that other factors, such as extinction and metallicity, are not likely to be the major

contributor of the broader color distribution of clumps. The difference of the E(B-V) distributions of clumps and "disks" is not significant, as can be seen from the bottom left panel of Figure 5. The mean and standard deviation of the E(B-V) distribution of clumps are 0.31 and 0.11, while those of "disks" are 0.27 and 0.10. The differences of both mean and standard deviation of the two components are actually smaller than the typical uncertainty of our E(B-V) measurement ($\sim$0.05). Although a few clumps do have very high dust extinctions, the insignificant difference between the E(B-V) distributions of clumps and "disks" suggests that extinction is not a major contributor of the broader color distribution of clumps. Another possible reason of the broad color distribution of clumps is the metallicity variation among clumps. Since metallicity is not a free parameter in our SED-fitting, we cannot draw conclusions on the metallicity distribution of clumps. Instead, we will discuss the effect of metallicity variation in Sec. 5.4.

A more significant difference between clumps and "disks" comes from the distributions of their projected stellar mass densities. The high resolution of ACS z-band images allows us to resolve each clump and hence measure its projected stellar density. By comparing the FWHM of clumps (after subtracting diffuse background) to that of ACS z-band PSF, we find that all our clumps except one are (marginally) resolved in the ACS z-band image. The fraction of resolved clumps in our sample is higher than that in Förster Schreiber et al. (2011), who found 18 out of 27 of their NIC2 clumps are resolved. The higher fraction of resolved clumps in our study can be explained by the higher resolution of ACS z-band image ($0.12''$), compared to that of NICMOS NIC2 images ($0.15''$). However, we also caution that the measurements of the projected stellar density of clumps in our study may suffer from systematical uncertainty, because the size of clumps is not precisely determined. To do so requires a detailed investigation on the light profiles of clumps and their host galaxies simultaneously. In this work, instead, we simply use the size of the apertures that we use to measure photometry as the size of clumps. The size is about two times the FWHM of H-band PSF, equivalent to about 5σ of the PSF, and is believed to be a good representative of clump sizes. The projected stellar density measured with this size can be treated as an average density of a clump.

The bottom right panel of Figure 5 shows that clumps are on average eight times denser than "disks". This result is non-trivial, because we identify clumps based on z-band images, which, observing the rest-frame UV light, is more sensitive to star formation than to stellar mass. Identified as prominent substructures in the z-band images, these clumps are expected to have active star formation but not necessarily to be denser. Using the light from both rest-frame UV and optical bands, our SED-fitting method turns out to show that clumps are regions with not only enhanced SSFRs but also more concentrated stellar distributions.

The higher stellar surface densities of clumps are consistent with the hypothetical scenario that clumps are formed through gravitational instabilities (e.g., Noguchi 1999; Immeli et al. 2004a,b; Bournaud et al. 2007, 2008; Elmegreen et al. 2008; Dekel et al. 2009b; Ceverino et al. 2010). Genzel et al. (2011) calculated the maps of Toomre Q-parameter for four galaxies in their sample and found that throughout the outer disks and toward the clumps, the Q-parameter is at or even significantly below unity. The small (<1) Q-parameter is evidence of gravitational instability. Since the total Q-parameter is inversely proportional to the sum of the molecular gas and stellar surface densities (see Eq. (2) of Genzel et al. (2011)), the regions with low Q-parameter (namely regions toward clumps) should have higher surface densities of gases and/or stars, as our results show. However, we remind that the possibility that the instability is driven by other violent

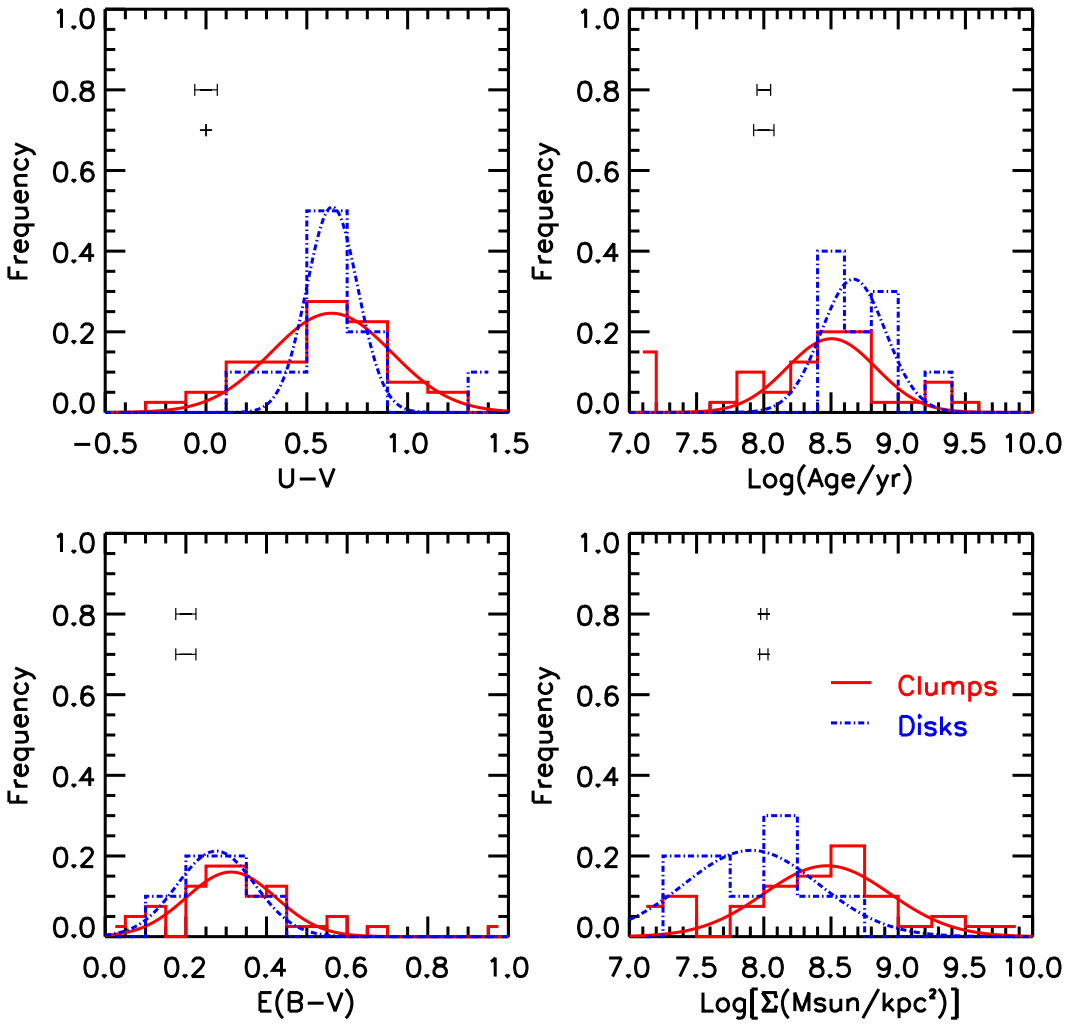

Fig. 5.— Comparisons between physical properties of clumps and their surrounding "disks". Red histograms show the distributions of properties of clumps, while blue those of "disks". Red and blue curves show the Gaussian fits to the red and blue histograms. Typical measurement errors are shown as horizontal error bars (upper for clumps and lower for "disks") in each panel.

processes, such as interaction or merger, cannot be ruled out simply based on the estimation of *Q*-parameter.

5. Clumps across Host Galaxies

In a widely held view, clumps are expected to migrate toward the gravitational centers of their host galaxies due to dynamical friction against the surrounding disks or clump interactions and eventually coalesce into a young bulge in several dynamical timescales ($\sim$0.5 Gyr) to form the progenitor of today's bulges. Alternatively, they could also be disrupted by either tidal force or stellar feedback to form part of a thick disk (e.g., Escala & Larson 2008; Dekel et al. 2009b). If clumps are able to survive the several dynamical timescales of migration, they are expected to exhibit a broad age dispersion, with older clumps generally closer to the galactic centers. Moreover, other physical properties of clumps would also change as the clumps migrate toward the galactic centers. For example, the gas outflows, as observed by Genzel et al. (2011), would be sufficiently strong to expel a large fraction of gas of clumps so that clumps are expected to become less efficient at forming stars when sinking toward centers. In this section, to understand the evolution of clumps, we study the radial variations of colors and physical properties of clumps along their host galaxies. We also discuss the effect of diffuse background subtraction (see Sec. 3) on our results. We will also discuss the possibility of metallicity variation as an explanation of the observed color radial variation.

5.1. Radial Variation of Color

Figure 6 shows the radial variation of the rest-frame U-V color of clumps across the host galaxies. We use the H-band light-weighted centers of host galaxies to represent the galactic centers, as the H-band is closest to the peak of stellar emission in all available bands. We calculate the galactocentric distance of each clump in the following three ways and study the radial variation in each case, respectively: (1) projected distance, scaled by the H-band Kron radius of its host galaxy (left panel); (2) deprojected distance, scaled by the Kron radius (middle panel); and (3) deprojected physical distance, in unit of kpc (right panel). All panels show a clear trend that clumps close to the centers of their host galaxies have redder rest-frame UV/optical colors than those in the outskirts. Although the slope of the radial color variation (or color gradient), defined as $\alpha = \Delta(U-V)/\Delta Log(R)$, varies with the definition of the galactocentric distance, it is significant beyond the 3σ confidence level in all cases (the values of the slope can be read from Figure 6). Therefore, we conclude that the radial color variation is an intrinsic feature of clumps and not affected by the distance definition. In later analysis, we use the scaled projected distance, as it gives us the strongest signal of radial variation and is independent of the assumption of the circle configuration of galaxies, which is used in our calculation of the deprojected distance, but still very uncertain for our galaxies. With the projected distance, the average colors of clumps become redder by 0.8 mag from radius of 0.7 $\mathrm{r_{Kron}}$ to 0.07 $\mathrm{r_{Kron}}$. This picture is broadly consistent with the scenario of inward migration of clumps. However, since the color is governed by a few factors: age, dust extinction and metallicity, the radial variation of color itself only provides an indirect comparison with theoretical hypothesis. The radial variations of physical properties are needed to make a direct comparison with models.

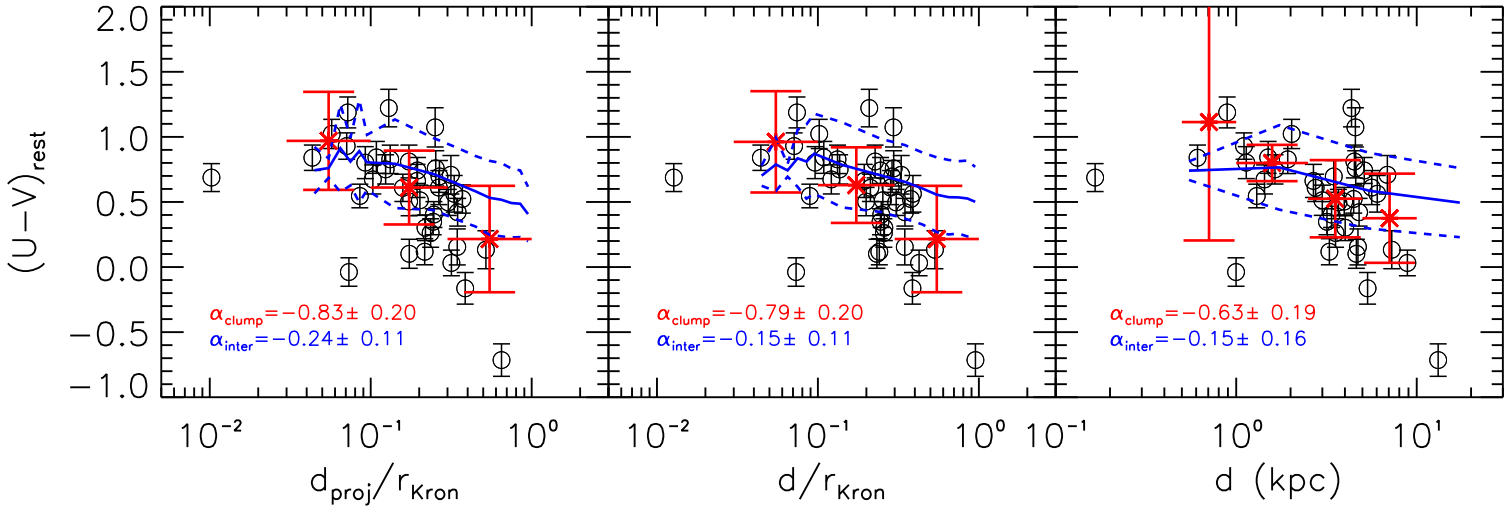

Fig. 6.— Radial variation of the rest-frame U-V color of clumps as a function of their galactocentric distances to the H-band light-weighted centers of their host galaxies. The distance is calculated in different ways in the three panels. *Left*: The distance is the projected distance, scaled by the H-band Kron radius of the host galaxy. *Middle*: It is the deprojected distance, scaled by the H-band Kron radius of the host galaxy. *Right*: It is the deprojected physical distance, in unit of kpc. To calculate the deprojected distance, we assume a circle configuration with the inclination angle equal to the axis ratio for each galaxy. In all panels, each circle with error bar stands for one clump. The red stars and red vertical error bars show the mean and 1σ deviation (after 3σ-clipping) of the clumps in each distance bin, while the bin size is shown by the red horizontal error bar. The solid and dashed blue lines in each panel show the mean and standard deviation of color variation of interclump pixels of all galaxies. The best-fit slope of the color gradients of clumps and interclump pixels are given in each panel.

There is one more issue that may also complicate the inference of the nature and fate of clumps from color variation and invalidate the inward migration scenario. It is the radial color variation of the diffuse components ("disk") of our galaxies. If the "disks" exhibit the same radial color variation (or gradient), it is then very likely that clumps are formed and, after that, stay in the locations where they are observed today. In this case, the radial variation of clumps can be explained by the radial variation of their host "disks", because thus formed clumps would have the same dust extinction and/or metallicity as that of their birthplaces in the host "disks". In order to examine the possible color gradient of host "disks", we measure the rest-frame U-V color of all interclump pixels (defined as pixels that are 0.3″ away from the center of any clumps) and study their radial variation. The mean and standard deviation of the color of interclump pixels are shown as a function of galactocentric distances in Figure 6. Interclump pixels show the similar trend of color gradient as clumps: red in center and blue in outskirts. However, the slope of the color gradient of interclump pixels (α_{inter}) is significant at only 2σ level with the rescaled projected galactocentric distance, and decreases to even only 1σ level with the deprojected physical distance, indicating a mild color gradient. More importantly, α_{inter} is significantly, at least at 3σ level, larger (flatter) than α_{clump}, the slope of the color gradient of clumps. The values of α_{inter} and α_{clump} can be read from Figure 6. The significant difference between the two slopes suggests that (1) the color gradient of "disks" can only explain a small part of the color gradient of clumps and (2) the formation and evolution of clumps are somehow dynamically separated from those of "disks". Therefore, a mechanism such as the inward migration is needed to explain the steeper gradient of clumps.

5.2. Radial Variations of Physical Properties

Figure 7 shows the radial variations of SSFR (top left), age (top right), E(B-V) (bottom left) and stellar surface density (bottom right) of clumps. Same as in Figure 6, the galactocentric distances of clumps are scaled by the H-band $\mathrm{r_{Kron}}$ of host galaxies. Clumps close to the centers of host galaxies have lower SSFRs, older ages, higher dust extinctions and higher stellar surface densities. On average, clumps located at $\mathrm{d} = \mathrm{d_{proj}}/\mathrm{r_{Kron}} < 0.1$ have four or five times lower SSFR than those at $\mathrm{d} > 0.5$. The average age of clumps at $\mathrm{d} > 0.5$ is about 100 Myr, while that of those at $\mathrm{d} < 0.1$ is about 700 Myr. The trend of E(B-V) is mild, increasing only 0.2 from $\mathrm{d} > 0.5$ to $\mathrm{d} < 0.1$. The stellar surface density changes dramatically, increasing about 25 times from $\mathrm{d} > 0.5$ to $\mathrm{d} < 0.1$.

As we discuss in Sec. 5.1, the host "disks" show a mild color gradient, which may contribute a small fraction of the observed radial color variation of clumps. Here we try to examine the implication of this color gradient on the possible gradient of physical properties of "disks". In order to do so, we have to run SED-fitting in each interclump pixel. However, the large photometric uncertainties of interclump pixels, especially of those in HST/ACS bands due to the relative low rest-frame UV emission of the diffuse components (as one can infer from Figure 1), prevent us from getting reliable fitting results for individual interclump pixels. In our study, we take a detour by assuming the (U-V) color–extinction relation and the color–age relation of each interclump pixel follow those of the integrated "disks". Thus, we extrapolate these relations of "disks" to the color of individual interclump pixels to obtain an estimation of the extinc-

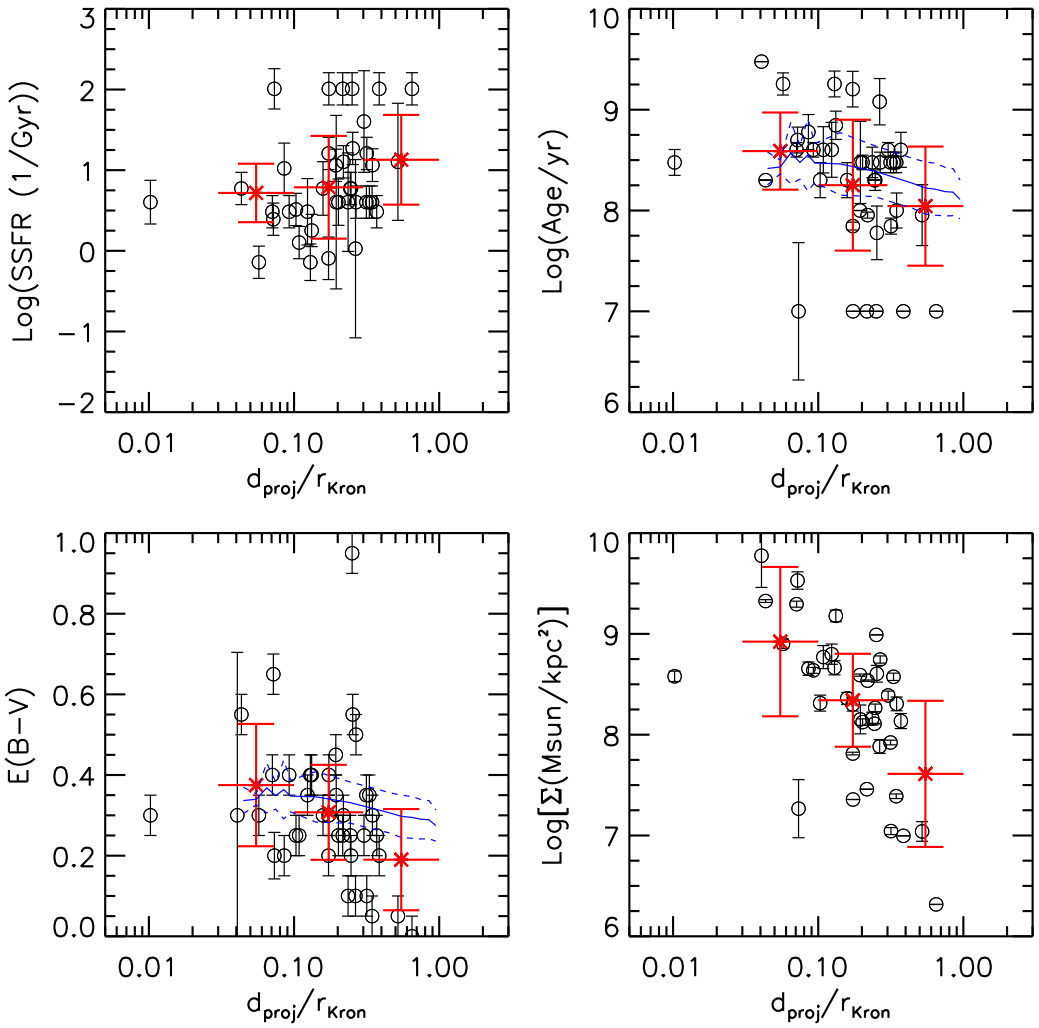

Fig. 7.— Radial variation of physical properties of clumps as a function of galactocentric distance. Symbols and colors are same as those in Figure 6.

tion and age of the pixels. We believe that such extrapolation is valid because the "disk" is the integration of all interclump pixels and hence represents the average color–extinction and color–age relations of the pixels.

The age and extinction gradients of interclump pixels are shown in Figure 7. Similar to the case of color gradient, both gradients are mild and cannot fully explain the observed radial variation of clump properties. The age gradient of interclump pixels varies only from ∼300 Myr at the projected galactocentric distance of ∼0.07 $\mathrm{r_{Kron}}$ to ∼100 at ∼1 $\mathrm{r_{Kron}}$, while a large fraction of clumps are found to have age >700 Myr at ∼0.07 $\mathrm{r_{Kron}}$ or to have age <100 Myr at ∼1 $\mathrm{r_{Kron}}$. The extinction of interclump pixels varies only by $\Delta \mathrm{E(B-V)} \sim 0.1$ throughout the "disks", while that of clumps varies by $\Delta \mathrm{E(B-V)} \sim 0.2$ from galactic centers to outskirts. Although not surprising, these results again demonstrate that the observed radial variations (or gradient) of clump properties are not a simple reflection the gradient of "disks". Clumps have their intrinsic radial variations so that their formation and evolution are separated from those of "disks", as discussed in Sec. 5.1.

The trends of these physical properties are consistent with the scenario of clumps migrating toward galactic centers in timescales of $\lesssim$1 Gyr. The trend of SSFR indicates that if the scenario is true, the intensity of star formation activity in clumps reduces as they migrate toward the gravitational centers. The reason of lower SSFR toward centers could be the gas outflow from massive clumps (Genzel et al. 2011). However, the outflow is not strong enough to fully quench the star formation in clumps, because even for clumps that are closest to galactic centers, their SSFRs are still several ten times higher than the usually quoted value for quiescent galaxies ($10^{-2}\mathrm{yr}^{-1}$).

The trends of age and E(B-V) are actually coupled due to the age–extinction degeneracy. Both high extinction and old age can be used to explain the relative red color of central clumps. To break the degeneracy requires resolved rest-frame NIR images, which unfortunately are not available to date. In our results, both parameters are partly responsible for the relative red color of central clumps. This shared responsibility could be real or just a reflection of the degeneracy. If the latter, using a sole parameter to explain the trend of U-V colors of clumps requires the trend of the parameter being even more prominent than what we see in the figure. That is, central clumps could be even older or more obscured. However, neither of the two situations is likely to be true. First, the stellar feedback would expel gas out of clumps as well as disrupt dust grains. The timescale of disrupting dust grains is much shorter than that of expelling gas and quenching star formation (Draine 2009). As a result, it is unlikely to find clumps with very high dust extinctions (E(B-V)>0.6) but low SSFRs toward the gravitational centers of host galaxies. Second, the ages of central clumps are already around 1 Gyr in the figure. A more prominent age trend would result in an average age of 2 Gyr or even older. It is hard to explain why these clumps were formed so early but have not fully migrated into the centers of galaxies to form bulges. Therefore, we conclude that both age and extinction should be responsible for the relative red color of central clumps.

5.3. Effect of Diffuse Background Subtraction

As described in Sec. 3, we subtract a *constant* diffuse background for all clumps in each galaxy. The real diffuse or "disk" component of a galaxy, however, is unlikely to have a constant profile, but instead to have a non-constant (e.g., exponential disk) profile. The simplified assumption of *constant* background would result in an over-subtraction for clumps in outskirts and an under-subtraction for central clumps. This problem exists for all bands but is more sever for red bands (e.g., H-band), since the background–clump contrast in the red band images is lower than that in blue band images, as one can infer from the z-band and H-band images in Figure 1. Therefore, the imperfect subtraction on diffuse background would redden the color of central clumps and blue the color of clumps in outskirts, inducing a false signal on the trend of radial variation of color in Figure 6 and subsequently on the trend of radial variations of physical properties in Figure 7.

Accurate subtraction of diffuse background is complicated. It requires knowledge on the light profile of underlying "disk" components of host galaxies. The commonly used method to obtain the light profile is fitting galaxy image with a Sérsic profile. Unfortunately, the image fitting technique has a few shortcomings: model dependent, not suitable for asymmetric source, and affected by the existence of clumps, which make it problematic for determining the underlying components of high redshift irregular-like clumpy galaxies in our sample. Elmegreen et al. (2009a) neglected the contribution of diffuse background when they studied the clumps in HUDF. This seems reasonable for their study, because they only used HST/ACS optical images, where the background–clump contrast is high so that the flux of clumps is 2–4 times higher than their surroundings.

In another study, Förster Schreiber et al. (2011) subtracted background from their NIC2 H-band images of clumpy galaxies and explored the impact of different background-subtraction schemes, including the one of no subtraction, on their results. They tracked the light profile of clumps until an upturn or a break appears and then used the surface brightness of the upturn or break as the surface brightness of local diffuse background. For clumps without an upturn or break, they measured the background just outside the photometric apertures of clumps. This method is sensible, but somehow subject to the determination of the upturn or break in a smoothly changing light profile, which may vary from person to person. Moreover, subtracting values from the upturns or from pixels just outside the clump photometric apertures would result in an over-subtraction, because (1) the upturn is more likely to be caused by the overlapping of two nearby clumps rather than by the domination of background and (2) there is no reason that the background would immediately dominate the flux just outside the photometric apertures of clumps. This possible over-subtraction could partly explain their findings that the local background light is typically 3–4 times higher than the background-subtracted clump fluxes, while in our study, the background only accounts for on average a few tens percent of the raw clump fluxes, with few of $\gtrsim$50%. Förster Schreiber et al. (2011) also estimated the uncertainty on the clump light contributions due to background subtraction by comparing the background-subtracted results with two other measurement methods: directly PSF measurement and raw photometry measurement without subtraction. They found that the clump light contributions are uncertain to a factor of $\sim$3. More importantly, one of their intriguing results, namely the trends of redder colors and of older ages for clumps at smaller galactocentric radii, is not significantly changed by using either background-subtracted

or raw photometry.

Since the background subtraction scheme would most affect the radial variations of color and physical properties of clumps, we investigate these variations in another two subtraction schemes: local subtraction and no subtraction at all. In the *local* subtraction scheme, for each clump, we measure the background surface brightness in an annulet that is $0.3''$(two times the radius of our photometry aperture) away from the clump, with all areas within a distance of $0.3''$of any other clumps masked out. Then, we subtract a corresponding background flux from the raw flux of the clump. In the *zero* scheme, we do not subtract any background from the raw fluxes of the clumps. We re-derive the rest-frame colors and physical properties of the clumps and re-analyze their radial variations. The new results are shown in Figure 8 for rest-frame UV/optical color and Figure 9 for physical properties and compared with the results of a global *constant* subtraction.

In both new subtraction schemes, the trend of the radial color variation is still present, although being flattened slightly: the difference between the average color of clumps at $\mathrm{d} < 0.1$ and $\mathrm{d} > 0.5$ becomes from 0.8 mag in the *constant* subtraction (black) to 0.5 mag in the *local* (blue) or the *zero* subtraction (red). As discussed above, the constant background subtraction scheme may over-subtract light, especially red light, from clumps in the outskirts, resulting in a false bluer color for them. However, in the other side, the zero background subtraction leaves the background light in red bands to these outskirts clumps, which would result in a false redder color for them. The real trend of the color radial variation should be the one between the constant subtraction and zero subtraction, most likely the local subtraction. We also note that the color of clumps in $\mathrm{d} < 0.1$ is not significantly changed in our zero subtraction scheme, implying that background emission is negligible for central clumps. Overall, the change of the color variation under different subtraction schemes is no statistically significant. Therefore, we conclude that the observed trend of color variation is intrinsic for clumps.

As we discussed in Sec. 5.1, the host "disks" exhibit a mild color gradient. It is important to examine whether the radial variation of clumps under different background subtraction is still significant steeper than that of interclump pixels. Since the background subtraction does not affect the gradient of interclump pixels (as discussed before, we exclude all pixels close to identified clumps), we simply overplot their color gradient obtained in Sec. 5.1 in Figure 8 (green) and compare its slope with that of clumps under various background subtraction schemes. The slope of clumps in the *zero* background subtraction is only steeper than that of interclump pixels at 2.4σ level. However, as discussed above, this trend, suffering from under-subtraction of diffuse background, can only be treated as the lower limit of the color gradient of clumps. The most likely color gradient of clumps, i.e., the one with *local* background subtraction, is 3.7σ steeper than that of interclump pixels. Thus, we conclude that the subtraction schemes of the diffuse background would not change our previous conclusion that the color gradient of "disks" is significantly flatter/weaker than, and hence only contribute to a small part of, that of clumps.

The radial variations for physical properties under different subtraction schemes are shown in Figure 9. The situation here is similar to that of Figure 8: all trends are still present, but with strength reduced. The trend of SSFR is reduced the most and only shows a marginal signal that clumps at $\mathrm{d} > 0.5$ are only

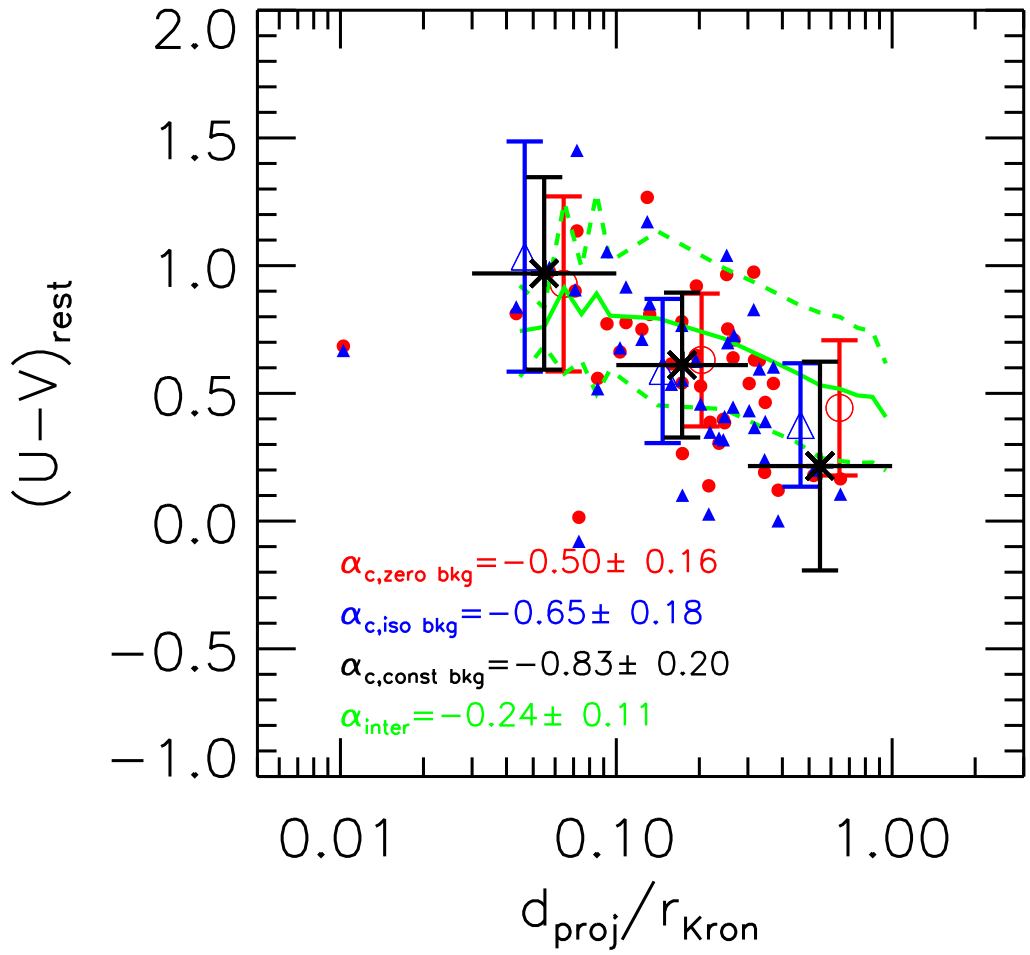

Fig. 8.— Radial variation of the rest-frame U-V color of clumps as a function of their galactocentric distances, under different schemes of diffuse background subtraction. Small filled blue triangles show the case of *local* background subtraction, while red circles show that of *zero* background subtraction. Large empty blue triangles (red circles) with error bars show the mean and 1σ deviation of the small filled blue triangles (red circles). Black "X" with error bars, identical to the red symbols in Figure 6, show the mean and 1σ deviation of the case that a global *constant* background is subtracted. Large empty blue triangles (red circles) are shifted along the x-axis for clarity. The typical color uncertainty of each clump is not shown, but can be inferred from the uncertainty of Figure 6. Solid and dashed green lines show the mean and standard deviation of color variation of interclump pixels. The best-fit slope of each color gradient is also given in the figure.

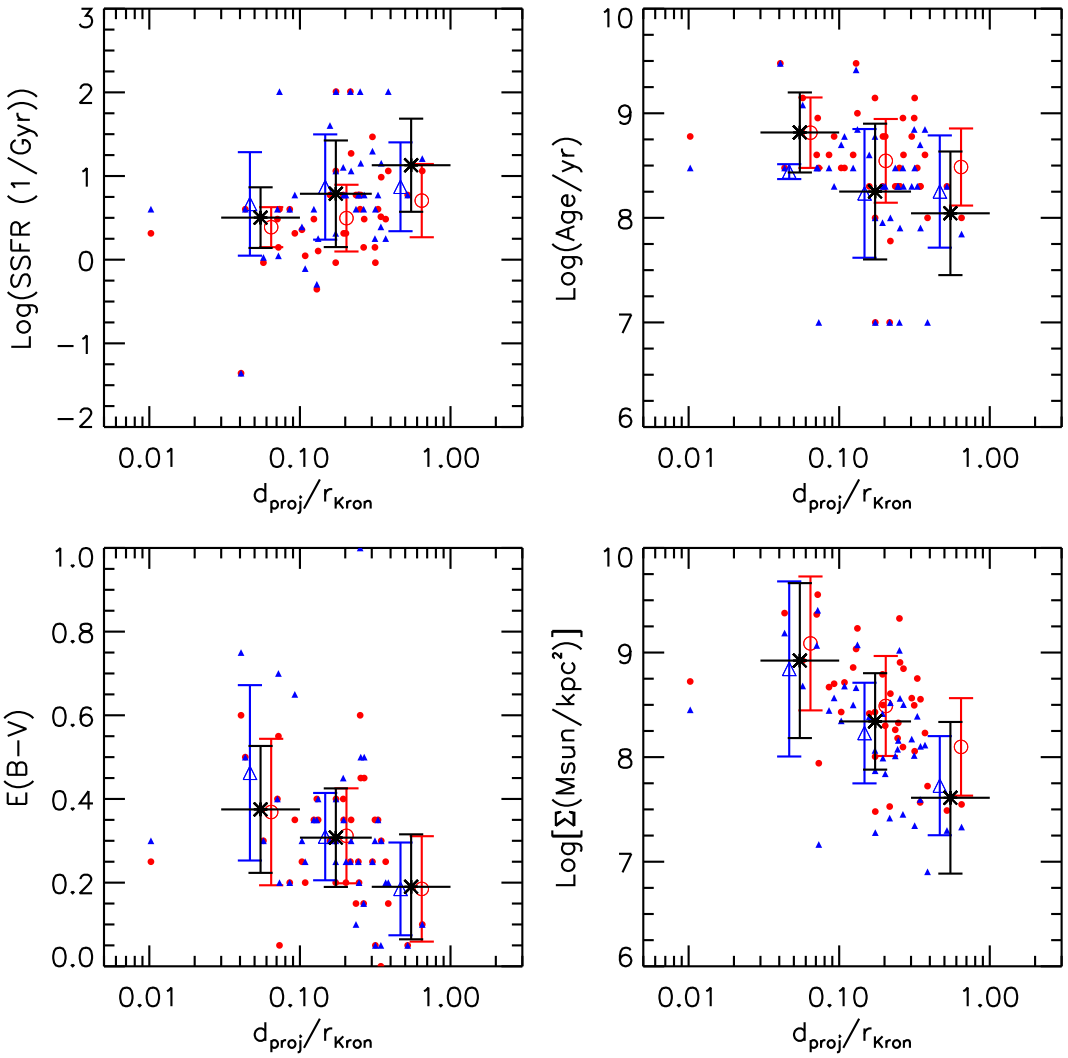

Fig. 9.— Radial variation of physical properties of clumps as a function of galactocentric distance, under different schemes of diffuse background subtraction. Symbols and colors are same as those in Figure 8.

a 1.5–2 times higher than those at $\mathrm{d} < 0.1$. The average age of clumps at $\mathrm{d} > 0.5$ increases from 100 Myr to 300 Myr so that the age difference between $\mathrm{d} < 0.1$ and $\mathrm{d} < 0.1$ reduces from >500 Myr of Figure 7 to ∼300 Myr. The trend of dust extinction is almost unchanged, implying that the E(B-V) measurement is statistically robust against background subtraction. The trend of the stellar surface density is also flattened, but still significant, even compared with the trend in Figure 7. The stellar surface densities of central clumps are now on average 10 times higher than that of clumps in outskirts.

Similar as for the color, the changes of above trends on physical properties are largely caused by the change of the derived properties of clumps in outskirts. On the other side, properties of central clumps are less (almost not) affected by the employed background subtraction schemes. Compared to the extreme case of over-subtraction due to the assumption of constant background, the zero subtraction is another extreme case for clumps in outskirts. The real diffuse background should be somewhere between these two cases. If the correct background is subtracted for these clumps, we would expect the radial variations of color and physical properties be stronger than those under the zero subtraction, but weaker than those under the constant subtraction. Overall, we can still conclude that central clumps are redder, older, denser, more obscured, and less active in forming stars than clumps in outskirts.

5.4. Possible Metallicity Variation

Our above analyses are based on our SED-fitting assumption that all clumps have solar metallicity. However, if there is a radial trend in metallicity (rich center and poor outskirts) already in place in the underlying disk, clumps that form closer to the center would tend to be redder, and vice versa. The radial variations due to the underlying metallicity gradient might mimic the color trends expected from the clump migration scenario.

The spatial variation in metallicity is indeed observed in clumpy SFGs at z∼2. Genzel et al. (2008) found that three out of five their SINS galaxies exhibits a radial gradient of the [N II]/Hα ratio, which implies a ∼20% higher oxygen metallicity in the central region than in the outer disks. Furthermore, Genzel et al. (2011) found clump to clump and center to outer variation in the [N II]/Hα ratio in another three SFGs at z∼2. These findings are broadly consistent with the inside–out growth mode predicted by semi-analytic models (e.g., Somerville et al. 2008). However, we note that the metallicity variation in their works is modest though. For example, the average metallicity among the three galaxies increases from ∼0.5 $Z_{\odot}$ in outer disks to ∼0.8 $Z_{\odot}$ in central regions.

Even if the above metallicity variation exists in our galaxies, its contribution to our observed color variation would be small. The rest-frame U-V color of a constant star-forming template with age of 1 Gyr changes only 0.2 mag from $Z = Z_{\odot}$ to $0.2Z_{\odot}$. However, in Figure 8, the radial color variation is $\gtrsim$0.6 mag, requiring other variations to explain it. We acknowledge the existence of metallicity variation, but still conclude that assuming a constant metallicity would not significantly affect our results on the radial variations of the SED-fitting derived properties. Moreover, the modest variation cannot be well constrained by SED-fitting, because the usually employed discrete metallicity distribution: sub-solar, solar, and super-

solar, is too broad to describe the variation.

6. Discussion

6.1. Comparisons with Other Studies

We compare our measurements of the properties of clumps with those of other studies. Due to the differences on a few key ingredients, e.g., sample selection, photometric apertures, background subtraction schemes, and models used to derive physical properties, only order-of-magnitude comparisons can be made. We focus on their stellar masses, SFRs and contributions to host galaxies. We are not able to compare clump sizes with other studies, as we fix a constant photometric apertures for all clumps. In order to compare stellar masses and SFRs that are derived with different IMFs, we apply the relation of Salimbeni et al. (2009b) to convert results with the Chabrier IMF Chabrier (2003) to that with the Salpeter IMF: $\log(\mathrm{M_{Salpeter}}) = \log(\mathrm{M_{Chabrier}}) + 0.24$. Since the normalization of SFR is determined by stellar mass in SED-fitting, we also scale the SED-fitting derived SFRs by a relation deduced from the above one: $\mathrm{SFR_{Salpeter}} = 1.74 \times \mathrm{SFR_{Chabrier}}$.

Since three galaxies in our sample (Galaxy 21739, 22284, and 27101) have been studied by Elmegreen & Elmegreen (2005), with ID 3465+, 3483, and 6462+ in their paper, we first compare the derived properties of these galaxies in the two studies in details, and then compare clump properties in sample wise with other studies. Table 3 shows the first comparison. As discussed in Sec. 2.2, Elmegreen & Elmegreen (2005) used ACS i-band to select clumpy galaxies and identified more clumps in each galaxy than we do. In order to derive physical parameters, including redshifts, of clumps as well as galaxies, Elmegreen & Elmegreen (2005) compare ACS color pairs of galaxies and clumps to that of stellar population synthesis models with exponentially decline SFH. Although the derived properties of clumps are different between the two studies and we are limited to a very small sample, we do not find systematical difference between the two studies for the following properties: average age of clumps, average stellar mass of clumps, stellar mass of host galaxies, and the fraction of mass in clumps.

The two parameters with obvious offsets between the two studies are the age of disks (called interclump age in Elmegreen & Elmegreen (2005)) and average SFR of clumps. The interclump age in Elmegreen & Elmegreen (2005) is $\sim$2 Gyr, while the disk age in our study is 0.3–0.5 Gyr. The difference could be due to the assumption of Elmegreen & Elmegreen (2005) that interclump star formation began at z=6. It could also be caused by the degeneracy between age (t) and the characteristic decay timescale (τ) in the SED-fitting of either of the two studies. However, the difference in the disk age would not change the results in both studies. Elmegreen & Elmegreen (2005) found that clumps are bluer than interclump regions, consistent with our conclusion that clumps are spots with enhanced SSFR. The systematical offset in the other parameter, the average SFR of clumps, is likely caused by the use of different SFR indicators in the two studies. Elmegreen & Elmegreen (2005) used the instantaneous SFR at a given time t, while we average the SFR over the last 100 Myr according to the SFH of the best-fit model. We argue that such average is necessary if one wants to compare the SFR derived from SED-fitting to that empirically derived the rest-

frame UV continuum, as the lifetime of O and B type stars is about 100 Myr. Since Elmegreen & Elmegreen (2005) used the exponentially declining model, such average will elevate the SFR of clumps from the instantaneous value of $\sim$1 $M_{\odot}yr^{-1}$ to several $M_{\odot}yr^{-1}$, consistent with our measurements. Overall, we conclude that the measurements of clump properties and, more importantly, the interpretation of the properties in the two studies are broadly consistent.

Now, we compare clump properties statistically in sample wise with other studies. The stellar masses of our clumps agree very well with those of Förster Schreiber et al. (2011), but are slightly larger those that of Elmegreen & Elmegreen (2005); Elmegreen et al. (2009a). The clumps in the NIC2 sample of Förster Schreiber et al. (2011) span the stellar mass range of $10^8M_{\odot}$ to $10^{10}M_{\odot}$, with a median mass of about $3 \times 10^9M_{\odot}$. Elmegreen & Elmegreen (2005) found a typical mass of $6 \times 10^8M_{\odot}$ for clumps in 10 HUDF galaxies. However, a revisit of HUDF by Elmegreen et al. (2009a) with NICMOS images shows that clumps are typically in range of $10^7M_{\odot}$ to $10^9M_{\odot}$. It is possible that the difference of stellar mass is resulted from sample selections. In our sample, we only choose galaxies with spectroscopic observations, which would bias our sample toward UV/optical luminous (and hence massive) end, while Elmegreen et al. (2009a) did not restrict their sample to spec-z and hence were able to detect clumps in fainter galaxies. As discussed in Genzel et al. (2011), the Toomre mass of clumps is proportional to the mass of disks. Clumps detected in our possibly biased massive samples would therefore have higher clump masses.

The SFRs of clumps in our study are broadly consistent with those of Genzel et al. (2011), who measured the SFRs of clumps through extinction corrected Hα luminosity. Their SFRs (after being converted to a Salpeter IMF) run from a few $M_{\odot}yr^{-1}$ to $\sim$70 $M_{\odot}yr^{-1}$, with a median (mean) of 24 (28) $M_{\odot}yr^{-1}$. In our sample, the SFRs of majority clumps cover a similarly wider range, from less than 1 $M_{\odot}yr^{-1}$ to $\sim$70 $M_{\odot}yr^{-1}$, with a median (mean) of $\sim$10 ($\sim$24) $M_{\odot}yr^{-1}$. The consistency of SFRs in the two studies is encouraging, because Genzel et al. (2011) and we have used two different physical mechanisms (nebular line emission and stellar color) to measure SFRs. Förster Schreiber et al. (2011) only measured SFR for galaxies as a whole. If we scale the SFRs of their host galaxies by the clump fractional contribution to H-band light in their study, typically 5%, the derived typical SFR of clumps is only a few $M_{\odot}yr^{-1}$, smaller than our median value. However, as we discussed in Sec. 4.3, as regions with enhanced SSFRs in "disks", clumps contribute more on SFR than on stellar mass (and hence H-band light) to host galaxies. Therefore, the actual SFRs in clumps of Förster Schreiber et al. (2011) should be higher than the above scaled value, moving them closer to our measurement. In fact, one galaxy (BX 482) in Förster Schreiber et al. (2011) has Hα measurement for each of its clumps. We calculate the Hα derived SFRs for each of its clumps. Since Förster Schreiber et al. (2011) did not report extinctions for individual clumps, we assume that the dust extinction of each clump is equal to the global extinction of BX 482, $A_V = 0.8$, measured through SED-fitting. We find that SFR varies from 5 $M_{\odot}yr^{-1}$ to 46 $M_{\odot}yr^{-1}$ for clumps in BX 482, with a median (mean) of 9 (14) $M_{\odot}yr^{-1}$, broadly consistent with our clump SFRs. Finally, we note that Hα is a measure of instantaneous SFR more than of the averaged SFR over the last 100 Myr, which we derive from our SED-fitting. The difference of the two SFR indicators may induce a bias when we compare the two types of SFRs. However, given the large uncertainties of measuring SFRs in both ways as well as the large scatter of SFRs of clumps, such a bias would not significantly affect our conclusions. SFRs measured through both Hα and SED-fitting on

larger samples are needed for carrying out more precise comparisons to better understand the star formation process in clumps.

In terms of fractional contribution of light to host galaxies, we compare our measurement on rest-frame UV/optical light to that on the observed emission of Förster Schreiber et al. (2011). At z$\sim$2, the rest-frame U and V band emissions are redshifted to close to the H_{160} and i_{814} bands in the observer's frame, validating the comparisons between the two papers. In our study, the typical individual clump contribution to the UV/Optical luminosity is $\sim$5% (spreading over a wide range of 1% to 10%) and the total contribution of clumps in a galaxy is $\sim$20%. We also find no significant difference between the clump contributions to U-band and V-band light. These results are quite similar to what Förster Schreiber et al. (2011) found with the H_{160} fluxes of their NIC2 clumps as well as i_{814} emission in one of their galaxy. The contribution on ACS i_{775} band emission by clumps in Elmegreen & Elmegreen (2005) and Elmegreen et al. (2009a) is typical 2%, slightly smaller than our average value. However, given that galaxies in Elmegreen & Elmegreen (2005) and Elmegreen et al. (2009a) usually contain 5–10 clumps, about two times more than our galaxies, the total contribution of clumps to host galaxies is about 25%, close to our value. Wuyts et al. (2012) found that the fractional contribution of clumps to the total light of their hosts has a mild dependence on the waveband used for identifying clumps, decreasing with the increasing of wavelength. They also found that for a giving identification band, the fractional contribution of clumps slightly decreases with wavelength. In their z$\sim$2 sample, the fractional contribution of clumps to the total rest-frame U (V) light of their hosts is, on average for detections in 2800Å, U, and V bands, 20% (17%), close to our values. However, we note that besides using a different sample selection criterion (mass-complete), Wuyts et al. (2012) have two other approaches that are different from ours: excluding the central bulge of a galaxy as a clump and not subtracting diffuse background of hosts from clump light, each of which brings an effect to the fractional contribution opposite to the other. These results again highlight the fact that the contribution of clumps to the total light of their host galaxies is small, and the light distributions of galaxies are still dominated by diffuse components.

6.2. Formation of Clumps

In the commonly assumed framework that giant clumps are formed through gravitational instability of turbulent gas-rich Toomre-unstable disks (e.g., Noguchi 1999; Immeli et al. 2004a,b; Bournaud et al. 2007, 2008; Elmegreen et al. 2008; Genzel et al. 2008; Dekel et al. 2009b; Ceverino et al. 2010; Genzel et al. 2011; Förster Schreiber et al. 2011), clumps have a characteristic scale and mass, namely the Toomre length and the Toomre mass. They represent the largest and fastest growing unstable mode that is not stabilized by rotation. Since we use a fix photometric aperture for all clumps, we lose the size information of clumps. However, we can still compare our clump masses with the Toomre mass predicted by the in-situ fragmentation scenario. We use Equation (5) in Genzel et al. (2011) to calculate the Toomre mass of disks:

$$M_{Toomre} \approx 5 \times 10^9 \left(\frac{f_{young}}{0.4}\right)^2 \left(\frac{M_{disk}}{10^{11} M_\odot}\right) M_\odot, \quad (1)$$

where f_{young} is the mass fraction of component of stars, and M_{disk} is the total mass of disk, which is close to the baryonic (gas + star) mass in the central $\sim$10 kpc of galaxies. The maximum clump mass that can be

formed in a uniformly rotationally supported gas disk is actually first derived by Escala & Larson (2008):

$$M_{cl}^{max} = 3 \times 10^7 M_\odot \left(\frac{\eta}{0.2}\right)^2 \left(\frac{M_{gas}}{10^9 M_\odot}\right), \quad (2)$$

where $\eta = M_{gas}/M_{tot}$ is the ratio of the gas mass to the total mass enclosed with a radius R. The maximum clump masses estimated by the two equations are in agreement within a factor of two. [1]

To apply Equation 1 to our galaxies, we assume a gas–to–baryonic mass fraction of 0.5, close to the median value of the fraction observed by several authors (e.g., Erb et al. 2006; Genzel et al. 2008; Tacconi et al. 2008, 2010; Förster Schreiber et al. 2009; Daddi et al. 2010). Therefore, we have $f_{young} = 0.5$ and M_{disk} is two times the stellar masses of the disks that are measured through SED-fitting. We compute the Toomre mass for each galaxy and compare the masses of clumps in the galaxy to the Toomre mass. The ratio between clump mass and Toomre mass spans a wide range, from 0.05 to 3.5, with a median of 0.3. This result is encouraging, as it demonstrates that our clump masses are broadly consistent with the characteristic mass predicted by the scenario of disk instability. The statistically smaller masses of clumps are not contradictory with the prediction, as the Toomre mass is the maximum unstable mass. Moreover, Toomre mass is proportional to the third power of gas density and inversely proportional to the forth power of angular rotation speed (see Equation (2) of Escala & Larson 2008). Since both gas density and angular rotation speed are functions of radius, the Toomre mass also varies with galactocentric distance. In a disk with flat rotation curve and gas density decreasing with radius, the Toomre mass decreases with radius. Our clump mass distribution is also consistent with this argument, as less dense (and hence less massive with given photometric aperture) clumps are found at large galactocentric distances. Overall, the clump masses in our sample are broadly consistent with the prediction of the scenario of gravitational instability.

The in-situ fragmentation due to gravitational instability requires a gas-rich, turbulent and marginally unstable ($Q \sim 1$) disk as the birthplace of clumps. The existence of such disks cannot be directly inferred from our multi-band images; it has to be confirmed through the kinematics of star, gas or ISM. Förster Schreiber et al. (2009) presented the spatially resolved gas kinematics of 62 star-forming galaxies at z$\sim$1–3, measured through Hα and [N II] emission lines observed by the Spectroscopic Imaging survey in the Near-infrared with SINFONI (SINS). They found that about one-third of galaxies in their sample are rotation-dominated yet turbulent disks, another one-third are compact and velocity dispersion-dominated objects, and the remaining one-third are interacting or merging systems. The also found that the fraction of rotation-dominated systems increases toward the massive end of the sample. Since almost all our galaxies have stellar mass larger than 10^{10}M$_\odot$ and lie on the massive end of the mass spectrum of SINS sample, we expect that the fraction of rotation-dominated turbulent disks in our sample is higher than 40%.

In fact, one galaxy in our sample, 27101, was observed by Bournaud et al. (2008) through Hα field spectroscopy using SINFONI on VLT UT4. They found a large-scale velocity gradient throughout the

[1] We note that the maximum clump mass is not the turbulent Jeans mass, which is often incorrectly interpreted in some of previous studies. The Jeans mass (and Jeans length), beyond which the disk cannot be stabilized purely by thermal pressure, is actually the smallest unstable mode that can be formed in a disk. We refer readers to Escala & Larson (2008) for detailed discussions.

system, with large local kinematic disturbances. They also found a disk-like radial metallicity gradient in the galaxy. These findings can be most likely explained by the scenario of internal disk fragmentation, despite the complex asymmetrical merger-like morphology. However, another galaxy in our sample, 24919, shows an obvious interaction/merger signature. A long (tidal) tail is curving from its lower left part all the way to its upper middle part, as can be seen in its z-band image in Figure 1, suggesting an ongoing interaction/merger, which might be responsible for the formation of clumps. To understand to which extension the in-situ fragmentation scenario is valid to explain the formation of giant clumps requires a large survey of kinematics of clumpy galaxies, in addition to their multi-band images.

Another possible interpretation of the clumpy features in our sample galaxies is that these clumps do not actually represent any physical entities, but simply correspond to locations with lower line-of-sight dust obscuration in the host galaxies. This alternative arises from the fact that these clumps are bright in the rest-frame UV images. If this interpretation is true, the properties (e.g., age and SSFR) and observed radial variations of clumps would plausibly reflect those of the underlying galaxy population. Based on our previous results, however, we argue that this alternative interpretation is unlikely true and that clumps are physical entities with properties and formations differing from those of their host "disks". For clumps in the outskirts (e.g., $r > 0.1r_{Kron}$) of galaxies, it is true that their dust obscuration is lower than that of interclump regions at the same galactocentric distance (the bottom left panel of Figure 7. However, these clumps also have systematically younger ages than their nearby interclump regions. The very young age ($\lesssim$100 Myr) of these clumps indicates that they are newly formed, possibly due to the instability induced by the cold accretion, which preferentially occurs in the outskirts of galaxies, in a relatively older (and hence stable) "disks". For central clumps, if they represented the underlying "disk" stellar populations but had lower dust extinction, their rest-frame colors should be *bluer* than their surrounding areas. However, this expectation is contradictory to our previous result, namely the rest-frame UV color of clumps is redder than that of central interclump regions (Figure 6). In fact, the bottom left panel of Figure 7 shows that the dust extinction of central clumps is comparable to (or even higher than) that of central "disk" regions, if our SED-fitting technique does not significantly suffer from the age–extinction degeneracy. Overall, it is unlikely that the appearance of the clump features is simply due to lower line-of-sight extinction. As a result, clumps should have origins distinctive from that of "disk" stellar populations.

6.3. Fate of Clumps

There are two possible scenarios commonly proposed to explain the fate for giant clumps in z$\sim$2 SFGs: they would (1) migrate toward the gravitational centers of their host galaxies due to interactions and dynamical friction against the surrounding disks and eventually coalesce into a young bulge as the progenitor of today's bulges or (2) be rapidly disrupted by stellar feedback, supernova feedback, or tidal torques during (or even before the beginning of) their migration toward centers. Dekel et al. (2009b) made a few predictions that observations can test for the possible fate of clumps. If the migration scenario is true and clumps survive for a migration timescale of $\sim$0.5 Gyr, giant clumps would (1) have an age spread of $\sim$0.5 Gyr; (2) be gas rich and forming stars at a high rate that is similar to the preceding few hundred Myr; and (3) have a radial

age variation in the sense that clumps at large disk radii are younger than $\sim$0.5 Gyr, while those at smaller radii are older. In contrast, if clumps are rapidly disrupted, they would (1) have smaller age spread, $\sim$100 Myr and (2) have no obvious age gradient with galactocentric radius.

Our findings on the properties of giant clumps are reasonably consistent with the prediction of the inward migration scenario. The top right panel of Figure 7 shows that the age distribution of our clumps spans a wide range from $<$0.1 Gyr to a few Gyr. The age spread is comparable to the prediction of $\sim$0.5 Gyr of the migration scenario, but significantly larger than the prediction ($\sim$ 100 Myr) of the disruption scenario. If no background subtraction is applied to our clumps, the age spread (see in Figure 9) is even closer to the prediction of the migration scenario. The radial age variation of our clumps is also strongly in favor of the migration scenario. Recently, Ceverino et al. (2012) discussed the internal support of the in-situ giant clumps in gravitationally unstable disks at high redshift, using both an analytic model and high-resolution hydro adaptive mesh refinement simulations. They predicted a steep age gradient of clumps throughout their host disk due to the formation of giant clumps in the outer parts of the disk and their inward migration to form a bulge in the disk center. Our results agree very well with their predictions: clumps at $d > 0.5$ have the mean age of $\sim$100 Myr, while those at $d < 0.1 \sim$ 700 Myr. Ceverino et al. (2012) even predicted that the age gradient of clumps is steeper than that of interclump stars. Such prediction is similar to our results in Figure 7 and hence strengthens our argument on the inward migration scenario. Another piece of evidence, interesting but largely uncertain, is coming from the SFH of clumps. As described in Sec. 3, we fit each clump with three types of SFHs: exponentially declining, exponentially increasing and constant. We then choose the most likely SFH based on the reduced χ^2 of the best-fit of each SFH. About 70%–80% of clumps are thus classified as having constant SFH, agreed with the above prediction of the migration scenario of Dekel et al. (2009b). However, we note that the SFH derived from SED-fitting is approximate and severely model dependent and can only be used as a loose constraint on predictions. Overall, we conclude that the age spread and radial variation indicate that these clumps might eventually migrate into the centers of their host galaxies.

It is also possible, however, that not all clumps can survive long enough to migrate into the gravitational centers. Some of them might still be disrupted, possibly by the stellar feedback (while the effect of supernovae feedback seems unimportant (see Dekel et al. (2009b))). Genzel et al. (2011) observed strong outflows in their clumps, with a rate as large as or even larger than SFRs. They also estimated the gas expulsion time due to outflows, which ranges from 170 to 1600 Myr from clump to clump. A hint of the disruption of clumps can also be inferred from the radial age variation of clumps (the top left panel of Figure 7 and Figure 9). In this figure, we find no clumps with age $\lesssim$100 Myr at small galactocentric radius ($d < 0.1$). The reason of the dearth of young central clumps could be either that young clumps are preferentially formed at large radii or that young clumps at small radii are rapidly disrupted due to the somehow stronger outflows or interactions. If the latter is true, the disruption timescale (or lifetime) of clumps should have a relation with the their densities, because due to their shallower potential wells and less concentrated structures, low density clumps are easier to be disrupted by either outflows or tidal torques than high density clumps.

Figure 10 shows that the age of clumps increases with the stellar surface densities of clumps. The upper envelope of the relation provides a rough estimate on the lifetime for clumps with different stellar surface

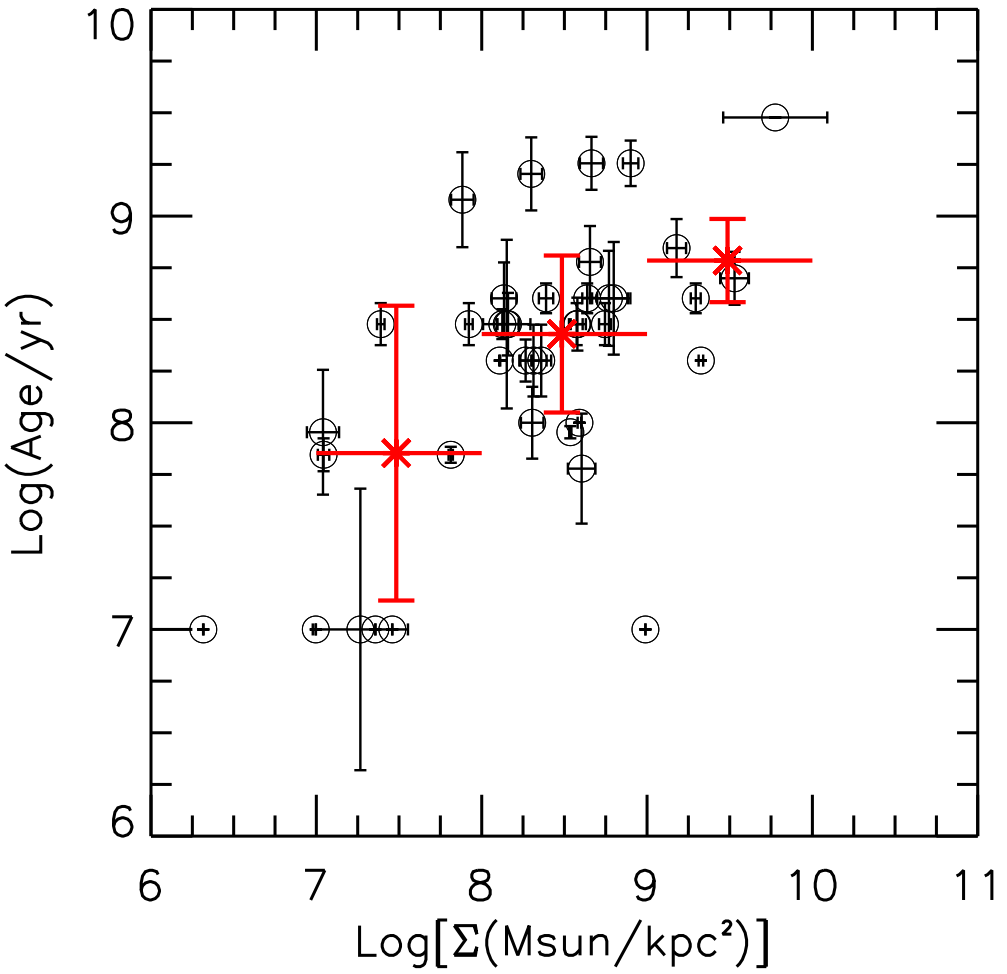

Fig. 10.— Age–stellar surface density relation of clumps. Symbols and colors are same as those in Figure 6. A constant background has been subtracted for clumps in this figure.

densities. For example, no clumps with density of $10^7 M_\odot/\mathrm{kpc}^2$ are older than 100 Myr, suggesting that the lifetime of this type of clumps is $\sim$100 Myr. While for clumps that are one order of magnitude denser, their lifetime could be up to 1 Gyr. However, we note that we cannot rule out an alternative scenario that all clumps are formed at large radii and become old and concentrated when they migrate toward galactic centers.

6.4. Ongoing Bulge Formation?

If the inward migration scenario is true, one would expect to find bulges or at least ongoing forming bulges in a fraction of z$\sim$2 SFGs. Clumps are observed within a wide redshift range, from z$\sim$4 (Elmegreen et al. 2007) to z$\sim$2 (e.g., Genzel et al. 2008, 2011; Förster Schreiber et al. 2011) or to even lower redshift. Moreover, very young clumps are observed at z$\sim$2 in our sample or other studies (e.g., Förster Schreiber et al. 2011). These observations show that the formation of clumps is a continuous process that at least lasts over the cosmic time of $\sim$1.7 Gyr from z$\sim$4 to z$\sim$2. If we assume a constant clump formation rate over the cosmic time and a bulge formation (due to the coalescent of clumps) timescale of 1 Gyr, a few times the migration timescale of clumps, the fraction of SFGs that contain a young bulge at z$\sim$2 should be (1.7-1)/1.7$\times$100%$\sim$40%. If the clump formation rate increases with redshift, the bulge fraction would be lower, as the majority of newly formed clumps have insufficient time to coalesce into bulges, and vice versa.

We roughly estimate the bulge fraction in our sample through the following ways:

1. *Morphology and color*: Bulges are believed to have spheroid-like morphology and be redder than other components if they are older. They also tend to reside in the gravitational centers of galaxies. By simply looking at the mosaics of our sample in Figure 1, we identify five galaxies (21852, 22284, 24033, 24684, 27101) that contain such a component that satisfies the above conditions. This bulge fraction (50%) is broadly consistent with what we estimated above based on the bulge formation timescale (40%). We note that although morphology and color are a relative easy way to identify bulges, they suffer from the age–dust degeneracy as well as the problem of subjectivity. A more accurate bulge identification requires other pieces of information, such as the kinematic information of bulges.

2. *Stellar mass*: As we discuss in Sec. 6.3, the Toomre mass is the maximum unstable mass that the Jeans-unstable mode not stabilized by rotation can generate. If the mass of a clump is far larger than the Toomre mass in its host disk, the clump may not be a direct result of disk fragmentation. Instead, it could be a coalesced result of a few clumps. In our study, a clump is considered a bulge if its stellar mass is three times larger than the Toomre mass. In our sample, four galaxies (23013, 24033, 24684, 27101) contain such super-Toomre mass clumps. Moreover, these super-Toomre mass clumps are all close to the H-band light centers — an approximation of the gravitational centers — of their host galaxies. This sub-sample is largely overlapped with the sub-sample that we identify through

morphology and color, with 3/4 of the former being in the latter. The bulge fraction of 40% measured in this way also agrees very well with our prediction. However, we note that using stellar and Toomre mass to set constraint on the bulge fraction critically relies on the accuracy and interpretation of the Toomre mass. Therefore, it can only be treated as a rough estimate.

3. *X-ray detection*: It is now widely accepted that super-massive black holes (SMBHs) are residing in the center of massive galaxies and co-evolve with bulges. The masses of SMBHs are observed to correlate strongly with both the fourth power of the velocity dispersion of bulges and the first power of the bulge masses. Also, recent theoretical models predict that the internal violent processes, such as clump–clump interaction, tidal force, etc., would feed gas to the center of galaxies to form bulges as well as SMBHs Bournaud et al. (2011). If bulges have been formed in our sample, we would expect some of our galaxies to be detected as AGN in X-ray due to the energetic feedback released by their accompanying SMBHs. Indeed, four galaxies (23013, 24684, 24919, 27101) in our sample have significant detections in the Chandra 4Ms imaging of CDFS[2], with three detected in both the soft and hard bands and one (27101) only in the soft band. At such high redshift (z$\sim$2), all these X-ray sources have high luminosities that can only be generated via AGN (Lx$> 10^{42}\,\mathrm{ergs}^{-1}$). This finding is encouraging, since this X-ray detected sub-sample is prominently overlapped with the super-Toomre mass sample that we just discussed above, with 3/4 of the former is found in the latter. The only exception, Galaxy 24919 shows an extraordinary red lane in its z-H color map. Regardless of the component of the lane, i.e., old stars or dust, its existence indicates that the galaxy is undergoing a dramatic violent process, possibly merger, a common way to form bulges. Including that, the bulge fraction inferred from X-ray detection is well agreed with our prediction of 40% as well as that induced from Toomre mass.

4. *Age*: Bulges should contain old stellar populations with ages older than a few times of the migration timescale of clumps ($\sim$0.5 Gyr). In our sample, only two galaxies (24686 and 27101) contain clumps with age older than 1 Gyr. Moreover, these clumps are very close to the centers of host galaxies. These findings indicate that these clumps could be bulges rather than newly formed clumps. The two galaxies also satisfy all above three criteria. Therefore, age provides the most restricted constraint on the bulge fraction and yields the smallest fraction (20%). However, we note that the age measured through SED-fitting is actually a light-weighted average age for both old and young population. In our clumps, since their SFRs have not been fully quenched, the new formed population would drag the measured age toward the young side. Therefore, some other clumps with age close but less than 1 Gyr may also contain populations as old as 1 Gyr and hence be candidates of proto-bulges.

Overall, our estimations yields a bulge fraction in our sample of z$\sim$2 clumpy galaxies from 50% through morphology and color to 20% through age. The most likely fraction of 40%, obtained by the prominent overlapping of super-Toomre mass and X-ray detection, is very close to our prediction based on

[2]http://cxc.harvard.edu/cda/Contrib/CDFS.html

the migration timescale of clumps. This result suggests that bulges have been likely formed through the coalescence of giant clumps in our sample of z∼2 clumpy galaxies and this process is still going on.

However, one should be cautionary when generalizing the conclusion to the general bulge formation of SFGs at z∼2. First, our sample is limited to only ten galaxies selected to be particularly clumpy and is biased toward UV bright, blue, and large galaxies, as discussed in Sec. 2.2. Second, our work cannot fully rule out other processes as the mechanisms of general bulge formation at z∼2. Genzel et al. (2008, 2011) studied the possible rapid disruption of clumps via vigorous outflows and the kinematic signatures of inward gas streaming motions in clumpy disks. These signatures suggest that the gas inflows that are fed to the centers of galaxies through internal violent processes may play an important role in building bulges along with clump migration, as highlighted in some of the most recent numerical simulations (e.g., Bournaud et al. 2011). Furthermore, given the fact that some objects in our sample may be merging systems, e.g., Galaxy 24919, the role of merger on building bulges cannot be fully excluded. It is very likely that more than one process could be responsible for early bulge building at z∼2. To understand the contribution of each possible mechanism requires further investigations with larger samples and newer observations.

7. Summary and Conclusion

In this paper, we study the properties of kpc-scale clumps in z∼2 SFGs through broad band multi-wavelength photometry. We identify clumps through a hybrid of auto-detection and visual inspection from ten galaxies with spec-z between 1.5 and 2.5 in the HUDF, where the recently available deep HST/WFC3 images, together with HST/ACS images, enable us to resolve into kpc-scale at z∼2 and detect clumps toward the faint end. Using the spatially resolved seven-band (BVizYJH) photometry, we measure physical properties of clumps through SED-fitting and allow the fitting to choose the best-fit parameters through three types of SFHs: exponentially decreasing, exponentially increasing, and constant. We also measure the properties of "disks", namely the diffuse components of the host galaxies. The main results of our paper are summarized as follows:

1. The number of clumps in our galaxies runs from 2 to 5, with a median of 4. The total number of 40 clumps enables us to study the physical properties of clumps with sufficient number statistics.

2. Most of our clumps have blue rest-frame UV–optical colors that are similar to the colors of their surrounding "disks" or their host galaxies as a whole. Only few clumps are as red as quiescent galaxies at z∼2. The CMD of clumps indicates that they are still actively forming stars.

3. The SFR–stellar mass relation of clumps and "disks" have almost the same slopes, but that of clumps has higher normalization, converting to higher SSFR. However, the SFR–stellar mass relation of the host galaxies as a whole is still dominated by "disk", as both SFR and stellar mass of host galaxies are largely contributed by "disks". This shows that clumps are regions with enhanced SSFR in "disks".

4. An individual clump typically contributes a few percent of the rest-frame UV/optical luminosity and stellar mass to its host galaxy. Together, all clumps in one galaxy typically contribute 20% of the

luminosity and stellar mass of the host galaxy. The contribution of clumps on SFR is higher, individually about 10% and together 50% of the host galaxies, consistent with the fact that clumps are regions with enhanced SSFR.

5. Clumps differ from their surrounding area in terms of age and stellar surface density. On average, clumps are younger by 0.2 dex and denser by eight times than their "disks". There is no obvious difference between the E(B-V) distributions of the two components. In terms of rest-frame U-V color, both components have similar median values, but clumps spread over a broader range, which may indicate the different SFHs or evolutionary stages of clumps.

6. Clumps have obvious radial variations on their properties. Clumps close to the centers of their host galaxies (the Kron radius scaled projected distance $d < 0.1$) are 0.7 mag redder in rest-frame U-V color than those in outskirts ($d > 0.5$). Spatially resolved SED-fitting shows that the color trend can be explained by the combination of radial variations of age and dust extinction. Central clumps ($d < 0.1$) are typically 600 Myr older and more extincted (E(B-V) larger by 0.2) than those in outskirts, with the latter is typically 100 Myr old and having E(B-V)$\sim$0.2. The central clumps are also 25 times denser than their outskirt counterparts. However, the trend of SSFR is slightly weak, only increasing by a factor of five from the central to outskirts.

7. The radial variations are affected by the scheme of diffuse background subtraction, but our conclusions are unaffected. Besides the above results with a *constant* background subtraction, we also study the radial variations under other two background subtraction schemes: *local* subtraction and *zero* subtraction. All the trends observed in the *constant* subtraction scheme are reserved in the two new cases of subtractions, but with strength weaken. The change of the strength is largely caused by the redder color of outskirt clumps in new subtraction schemes than in the *constant* subtraction scheme. The central clumps are now only 0.5 mag redder and 300 Myr older than outskirt clumps. The trend of E(B-V) does not significantly change. And the trend of stellar surface density is still prominent, with the central ones still 10 times denser than the outskirt ones. The SSFR trend is weaken the most, with a difference only a few times between centers and outskirts. Arguing that the real trends would reside between the two extreme cases of background subtraction: *constant* and *zero*, we conclude that central clumps are redder, older, more extincted, denser, and less active on forming stars than outskirt clumps.

8. The host "disks" (interclump regions) exhibit mild gradients of rest-frame UV color, age, and dust extinction. However, these gradients are significantly weaker/flatter than those of clumps. The results suggest that (1) the observed color and property gradients of clumps are not a simple reflection of those of host "disks"; (2) the color and property gradients of "disks" contribute to, if any, only a small part of the gradients of clumps; and (3) the evolution of clumps is dynamically separated from those of "disks". Thus, we claim that mechanisms such as the inward migration are needed to explain the steeper gradient of clumps. A further test also shows that the use of different background subtraction schemes does not significantly change this result.

9. Our measurements of the properties of clumps are broadly consistent with those of previous observational studies. They are also consistent with the clump formation mechanism that clumps are formed through gravitational instability in gas-rich turbulent disks, proposed by several theoretical work and numerical simulations. However, we cannot rule out the scenario that clumps are formed through external violent processes, e.g., interactions and mergers, as a couple of galaxies in our sample show merger signatures.

10. The obvious radial variations of clump properties, especially the radial age variation, are consistent with the hypothesis that clumps would migrate toward the centers of their host galaxies, with a timescale of $\sim$0.5 Gyr, and eventually coalesce into young bulges. However, the dearth of young clumps in the central regions of galaxies reminds us that not all clumps are able to survive enough to migrate into centers. We argue that the lifetime of clumps is correlated with their stellar surface densities. Only clumps that are dense enough can survive long enough to sink into the centers.

11. We roughly estimate whether some clumps in our sample are actually coalesced bulges or proto-bulges through a few ways: morphology and color of clumps, stellar mass of clumps, X-ray detection of galaxies, and age of clumps. The bulge fraction, namely the fraction of galaxies that contain bulges, in our sample is 20%–50%, depending on the way of constraint. This result is broadly consistent with the prediction based on the migration timescale of clumps. We argue that the process of bulge formation is ongoing in our z$\sim$2 sample.

We note that our sample only contains 10 galaxies and thus is likely subject to small number statistics incompleteness. Also, our results apply strictly to galaxies with relatively large UV luminosity, since our sample only includes cases with spectroscopic redshifts. In order to obtain a robust statistical characterization of the properties of clumps, including their dependence on radial separation from the center of the galaxies and the fraction of clumpy galaxies at z$\sim$2, a much larger sample covering a wider range of both luminosity and stellar mass is needed. The ongoing CANDELS (Grogin et al. 2011; Koekemoer et al. 2011) is beginning to provide deep images over a larger sky area, ≈ 0.5 square degree, to answer these questions. Moreover, the deep NIR observation of CANDELS will significantly improve the accuracy of the photometric redshift measurements at z$\sim$2, enabling us to construct deeper samples not limited by spec-z. Wuyts et al. (2012) already used part of CANDELS data to study the profiles of color, surface stellar mass density, age, and extinction of a large sample of massive SFGs and to address clump properties. Their approach is different from ours, as we try to identify clumps and separate the light and properties of clumps from those of the diffuse background of host galaxies, while they focused generally on regions with excess surface brightness and did not subtract the diffuse background light from clumps. Both approaches are complementary to each other and needed to obtain a robust view on the nature and fate of clumps. In a future paper we will report on a study similar to the one discussed in this paper that takes advantage of the CANDELS data set.

We thank the anonymous referee for constructive comments that improve this article.

REFERENCES

Beckwith, S. V. W., Stiavelli, M., Koekemoer, A. M., Caldwell, J. A. R., Ferguson, H. C., Hook, R., Lucas, R. A., Bergeron, L. E., Corbin, M., Jogee, S., Panagia, N., Robberto, M., Royle, P., Somerville, R. S., & Sosey, M. 2006, AJ, 132, 1729

Bell, E. F., Wolf, C., Meisenheimer, K., Rix, H.-W., Borch, A., Dye, S., Kleinheinrich, M., Wisotzki, L., & McIntosh, D. H. 2004, ApJ, 608, 752

Blanton, M. R., Hogg, D. W., Bahcall, N. A., Baldry, I. K., Brinkmann, J., Csabai, I., Eisenstein, D., Fukugita, M., Gunn, J. E., Ivezić, Ž., Lamb, D. Q., Lupton, R. H., Loveday, J., Munn, J. A., Nichol, R. C., Okamura, S., Schlegel, D. J., Shimasaku, K., Strauss, M. A., Vogeley, M. S., & Weinberg, D. H. 2003, ApJ, 594, 186

Bournaud, F., Daddi, E., Elmegreen, B. G., Elmegreen, D. M., Nesvadba, N., Vanzella, E., Di Matteo, P., Le Tiran, L., Lehnert, M., & Elbaz, D. 2008, A&A, 486, 741

Bournaud, F., Dekel, A., Teyssier, R., Cacciato, M., Daddi, E., Juneau, S., & Shankar, F. 2011, ApJ, 741, L33

Bournaud, F., Elmegreen, B. G., & Elmegreen, D. M. 2007, ApJ, 670, 237

Bournaud, F., Elmegreen, B. G., & Martig, M. 2009, ApJ, 707, L1

Bouwens, R. J., Illingworth, G. D., Oesch, P. A., Stiavelli, M., van Dokkum, P., Trenti, M., Magee, D., Labbé, I., Franx, M., Carollo, C. M., & Gonzalez, V. 2010, ApJ, 709, L133

Brammer, G. B., Whitaker, K. E., van Dokkum, P. G., Marchesini, D., Labbé, I., Franx, M., Kriek, M., Quadri, R. F., Illingworth, G., Lee, K.-S., Muzzin, A., & Rudnick, G. 2009, ApJ, 706, L173

Bruzual, G., & Charlot, S. 2003, MNRAS, 344, 1000

Cassata, P., Giavalisco, M., Guo, Y., Ferguson, H., Koekemoer, A. M., Renzini, A., Fontana, A., Salimbeni, S., Dickinson, M., Casertano, S., Conselice, C. J., Grogin, N., Lotz, J. M., Papovich, C., Lucas, R. A., Straughn, A., Gardner, J. P., & Moustakas, L. 2010, ApJ, 714, L79

Ceverino, D., Dekel, A., & Bournaud, F. 2010, MNRAS, 404, 2151

Ceverino, D., Dekel, A., Mandelker, N., Bournaud, F., Burkert, A., Genzel, R., & Primack, J. 2012, MNRAS, 420, 3490

Chabrier, G. 2003, PASP, 115, 763

Conselice, C. J., Grogin, N. A., Jogee, S., Lucas, R. A., Dahlen, T., de Mello, D., Gardner, J. P., Mobasher, B., & Ravindranath, S. 2004, ApJ, 600, L139

Conselice, C. J., Rajgor, S., & Myers, R. 2008, MNRAS, 386, 909

Cresci, G., Mannucci, F., Maiolino, R., Marconi, A., Gnerucci, A., & Magrini, L. 2010, Nature, 467, 811

Daddi, E., Bournaud, F., Walter, F., Dannerbauer, H., Carilli, C. L., Dickinson, M., Elbaz, D., Morrison, G. E., Riechers, D., Onodera, M., Salmi, F., Krips, M., & Stern, D. 2010, ApJ, 713, 686

Daddi, E., Dickinson, M., Morrison, G., Chary, R., Cimatti, A., Elbaz, D., Frayer, D., Renzini, A., Pope, A., Alexander, D. M., Bauer, F. E., Giavalisco, M., Huynh, M., Kurk, J., & Mignoli, M. 2007, ApJ, 670, 156

Daddi, E., Renzini, A., Pirzkal, N., Cimatti, A., Malhotra, S., Stiavelli, M., Xu, C., Pasquali, A., Rhoads, J. E., Brusa, M., di Serego Alighieri, S., Ferguson, H. C., Koekemoer, A. M., Moustakas, L. A., Panagia, N., & Windhorst, R. A. 2005, ApJ, 626, 680

Dahlen, T., Mobasher, B., Dickinson, M., Ferguson, H. C., Giavalisco, M., Grogin, N. A., Guo, Y., Koekemoer, A., Lee, K.-S., Lee, S.-K., Nonino, M., Riess, A. G., & Salimbeni, S. 2010, ApJ, 724, 425

Dekel, A., Birnboim, Y., Engel, G., Freundlich, J., Goerdt, T., Mumcuoglu, M., Neistein, E., Pichon, C., Teyssier, R., & Zinger, E. 2009a, Nature, 457, 451

Dekel, A., Sari, R., & Ceverino, D. 2009b, ApJ, 703, 785

Draine, B. T. 2009, in Astronomical Society of the Pacific Conference Series, Vol. 414, Astronomical Society of the Pacific Conference Series, ed. T. Henning, E. Grün, & J. Steinacker, 453–+

Elmegreen, B. G., Bournaud, F., & Elmegreen, D. M. 2008, ApJ, 688, 67

Elmegreen, B. G., & Elmegreen, D. M. 2005, ApJ, 627, 632

Elmegreen, B. G., Elmegreen, D. M., Fernandez, M. X., & Lemonias, J. J. 2009a, ApJ, 692, 12

Elmegreen, D. M., Elmegreen, B. G., Marcus, M. T., Shahinyan, K., Yau, A., & Petersen, M. 2009b, ApJ, 701, 306

Elmegreen, D. M., Elmegreen, B. G., Ravindranath, S., & Coe, D. A. 2007, ApJ, 658, 763

Erb, D. K., Steidel, C. C., Shapley, A. E., Pettini, M., Reddy, N. A., & Adelberger, K. L. 2006, ApJ, 646, 107

Escala, A., & Larson, R. B. 2008, ApJ, 685, L31

Förster Schreiber, N. M., Genzel, R., Bouché, N., Cresci, G., Davies, R., Buschkamp, P., Shapiro, K., Tacconi, L. J., Hicks, E. K. S., Genel, S., Shapley, A. E., Erb, D. K., Steidel, C. C., Lutz, D., Eisenhauer, F., Gillessen, S., Sternberg, A., Renzini, A., Cimatti, A., Daddi, E., Kurk, J., Lilly, S., Kong, X., Lehnert, M. D., Nesvadba, N., Verma, A., McCracken, H., Arimoto, N., Mignoli, M., & Onodera, M. 2009, ApJ, 706, 1364

Förster Schreiber, N. M., Shapley, A. E., Genzel, R., Bouché, N., Cresci, G., Davies, R., Erb, D. K., Genel, S., Lutz, D., Newman, S., Shapiro, K. L., Steidel, C. C., Sternberg, A., & Tacconi, L. J. 2011, ApJ, 739, 45

Franx, M., van Dokkum, P. G., Schreiber, N. M. F., Wuyts, S., Labbé, I., & Toft, S. 2008, ApJ, 688, 770

Gargiulo, A., Saracco, P., & Longhetti, M. 2011, MNRAS, 67

Genel, S., Naab, T., Genzel, R., Förster Schreiber, N. M., Sternberg, A., Oser, L., Johansson, P. H., Davé, R., Oppenheimer, B. D., & Burkert, A. 2012, ApJ, 745, 11

Genzel, R., Burkert, A., Bouché, N., Cresci, G., Förster Schreiber, N. M., Shapley, A., Shapiro, K., Tacconi, L. J., Buschkamp, P., Cimatti, A., Daddi, E., Davies, R., Eisenhauer, F., Erb, D. K., Genel, S., Gerhard, O., Hicks, E., Lutz, D., Naab, T., Ott, T., Rabien, S., Renzini, A., Steidel, C. C., Sternberg, A., & Lilly, S. J. 2008, ApJ, 687, 59

Genzel, R., Newman, S., Jones, T., Förster Schreiber, N. M., Shapiro, K., Genel, S., Lilly, S. J., Renzini, A., Tacconi, L. J., Bouché, N., Burkert, A., Cresci, G., Buschkamp, P., Carollo, C. M., Ceverino, D., Davies, R., Dekel, A., Eisenhauer, F., Hicks, E., Kurk, J., Lutz, D., Mancini, C., Naab, T., Peng, Y., Sternberg, A., Vergani, D., & Zamorani, G. 2011, ApJ, 733, 101

Giavalisco, M., Dickinson, M., Ferguson, H. C., Ravindranath, S., Kretchmer, C., Moustakas, L. A., Madau, P., Fall, S. M., Gardner, J. P., Livio, M., Papovich, C., Renzini, A., Spinrad, H., Stern, D., & Riess, A. 2004, ApJ, 600, L103

Giavalisco, M., Vanzella, E., Salimbeni, S., Tripp, T. M., Dickinson, M., Cassata, P., Renzini, A., Guo, Y., Ferguson, H. C., Nonino, M., Cimatti, A., Kurk, J., Mignoli, M., & Tang, Y. 2011, ApJ, 743, 95

Grazian, A., Salimbeni, S., Pentericci, L., Fontana, A., Nonino, M., Vanzella, E., Cristiani, S., de Santis, C., Gallozzi, S., Giallongo, E., & Santini, P. 2007, A&A, 465, 393

Grogin, N. A., Kocevski, D. D., Faber, S. M., Ferguson, H. C., Koekemoer, A. M., Riess, A. G., Acquaviva, V., Alexander, D. M., Almaini, O., Ashby, M. L. N., Barden, M., Bell, E. F., Bournaud, F., Brown, T. M., Caputi, K. I., Casertano, S., Cassata, P., Castellano, M., Challis, P., Chary, R.-R., Cheung, E., Cirasuolo, M., Conselice, C. J., Roshan Cooray, A., Croton, D. J., Daddi, E., Dahlen, T., Davé, R., de Mello, D. F., Dekel, A., Dickinson, M., Dolch, T., Donley, J. L., Dunlop, J. S., Dutton, A. A., Elbaz, D., Fazio, G. G., Filippenko, A. V., Finkelstein, S. L., Fontana, A., Gardner, J. P., Garnavich, P. M., Gawiser, E., Giavalisco, M., Grazian, A., Guo, Y., Hathi, N. P., Häussler, B., Hopkins, P. F., Huang, J.-S., Huang, K.-H., Jha, S. W., Kartaltepe, J. S., Kirshner, R. P., Koo, D. C., Lai, K., Lee, K.-S., Li, W., Lotz, J. M., Lucas, R. A., Madau, P., McCarthy, P. J., McGrath, E. J., McIntosh, D. H., McLure, R. J., Mobasher, B., Moustakas, L. A., Mozena, M., Nandra, K., Newman, J. A., Niemi, S.-M., Noeske, K. G., Papovich, C. J., Pentericci, L., Pope, A., Primack, J. R., Rajan, A., Ravindranath, S., Reddy, N. A., Renzini, A., Rix, H.-W., Robaina, A. R., Rodney, S. A., Rosario, D. J., Rosati, P., Salimbeni, S., Scarlata, C., Siana, B., Simard, L., Smidt, J., Somerville, R. S.,

Spinrad, H., Straughn, A. N., Strolger, L.-G., Telford, O., Teplitz, H. I., Trump, J. R., van der Wel, A., Villforth, C., Wechsler, R. H., Weiner, B. J., Wiklind, T., Wild, V., Wilson, G., Wuyts, S., Yan, H.-J., & Yun, M. S. 2011, ApJS, 197, 35

Guo, Y., Giavalisco, M., Cassata, P., Ferguson, H. C., Dickinson, M., Renzini, A., Koekemoer, A., Grogin, N. A., Papovich, C., Tundo, E., Fontana, A., Lotz, J. M., & Salimbeni, S. 2011, ApJ, 735, 18

Guo, Y., Giavalisco, M., Cassata, P., Ferguson, H. C., Williams, C. C., Dickinson, M., Koekemoer, A., Grogin, N. A., Chary, R.-R., Messias, H., Tundo, E., Lin, L., Lee, S.-K., Salimbeni, S., Fontana, A., Grazian, A., Kocevski, D., Lee, K.-S., Villanueva, E., & van der Wel, A. 2012, ApJ, 749, 149

Immeli, A., Samland, M., Gerhard, O., & Westera, P. 2004a, A&A, 413, 547

Immeli, A., Samland, M., Westera, P., & Gerhard, O. 2004b, ApJ, 611, 20

Jones, T. A., Swinbank, A. M., Ellis, R. S., Richard, J., & Stark, D. P. 2010, MNRAS, 404, 1247

Kereš, D., Katz, N., Weinberg, D. H., & Davé, R. 2005, MNRAS, 363, 2

Koekemoer, A. M., Faber, S. M., Ferguson, H. C., Grogin, N. A., Kocevski, D. D., Koo, D. C., Lai, K., Lotz, J. M., Lucas, R. A., McGrath, E. J., Ogaz, S., Rajan, A., Riess, A. G., Rodney, S. A., Strolger, L., Casertano, S., Castellano, M., Dahlen, T., Dickinson, M., Dolch, T., Fontana, A., Giavalisco, M., Grazian, A., Guo, Y., Hathi, N. P., Huang, K.-H., van der Wel, A., Yan, H.-J., Acquaviva, V., Alexander, D. M., Almaini, O., Ashby, M. L. N., Barden, M., Bell, E. F., Bournaud, F., Brown, T. M., Caputi, K. I., Cassata, P., Challis, P. J., Chary, R.-R., Cheung, E., Cirasuolo, M., Conselice, C. J., Roshan Cooray, A., Croton, D. J., Daddi, E., Davé, R., de Mello, D. F., de Ravel, L., Dekel, A., Donley, J. L., Dunlop, J. S., Dutton, A. A., Elbaz, D., Fazio, G. G., Filippenko, A. V., Finkelstein, S. L., Frazer, C., Gardner, J. P., Garnavich, P. M., Gawiser, E., Gruetzbauch, R., Hartley, W. G., Häussler, B., Herrington, J., Hopkins, P. F., Huang, J.-S., Jha, S. W., Johnson, A., Kartaltepe, J. S., Khostovan, A. A., Kirshner, R. P., Lani, C., Lee, K.-S., Li, W., Madau, P., McCarthy, P. J., McIntosh, D. H., McLure, R. J., McPartland, C., Mobasher, B., Moreira, H., Mortlock, A., Moustakas, L. A., Mozena, M., Nandra, K., Newman, J. A., Nielsen, J. L., Niemi, S., Noeske, K. G., Papovich, C. J., Pentericci, L., Pope, A., Primack, J. R., Ravindranath, S., Reddy, N. A., Renzini, A., Rix, H.-W., Robaina, A. R., Rosario, D. J., Rosati, P., Salimbeni, S., Scarlata, C., Siana, B., Simard, L., Smidt, J., Snyder, D., Somerville, R. S., Spinrad, H., Straughn, A. N., Telford, O., Teplitz, H. I., Trump, J. R., Vargas, C., Villforth, C., Wagner, C. R., Wandro, P., Wechsler, R. H., Weiner, B. J., Wiklind, T., Wild, V., Wilson, G., Wuyts, S., & Yun, M. S. 2011, ApJS, 197, 36

Laidler, V. G., Papovich, C., Grogin, N. A., Idzi, R., Dickinson, M., Ferguson, H. C., Hilbert, B., Clubb, K., & Ravindranath, S. 2007, PASP, 119, 1325

Lee, S., Ferguson, H. C., Somerville, R. S., Wiklind, T., & Giavalisco, M. 2010, ApJ, 725, 1644

Lee, S.-K., Idzi, R., Ferguson, H. C., Somerville, R. S., Wiklind, T., & Giavalisco, M. 2009, ApJS, 184, 100

Lotz, J. M., Madau, P., Giavalisco, M., Primack, J., & Ferguson, H. C. 2006, ApJ, 636, 592

Ly, C., Malkan, M. A., Hayashi, M., Motohara, K., Kashikawa, N., Shimasaku, K., Nagao, T., & Grady, C. 2011, ApJ, 735, 91

Maraston, C., Pforr, J., Renzini, A., Daddi, E., Dickinson, M., Cimatti, A., & Tonini, C. 2010, MNRAS, 407, 830

Mendez, A. J., Coil, A. L., Lotz, J., Salim, S., Moustakas, J., & Simard, L. 2011, ApJ, 736, 110

Murray, N., Quataert, E., & Thompson, T. A. 2010, ApJ, 709, 191

Noguchi, M. 1999, ApJ, 514, 77

Nonino, M., Dickinson, M., Rosati, P., Grazian, A., Reddy, N., Cristiani, S., Giavalisco, M., Kuntschner, H., Vanzella, E., Daddi, E., Fosbury, R. A. E., & Cesarsky, C. 2009, ApJS, 183, 244

Oesch, P. A., Bouwens, R. J., Illingworth, G. D., Carollo, C. M., Franx, M., Labbé, I., Magee, D., Stiavelli, M., Trenti, M., & van Dokkum, P. G. 2010, ApJ, 709, L16

Oesch, P. A., Stiavelli, M., Carollo, C. M., Bergeron, L. E., Koekemoer, A. M., Lucas, R. A., Pavlovsky, C. M., Trenti, M., Lilly, S. J., Beckwith, S. V. W., Dahlen, T., Ferguson, H. C., Gardner, J. P., Lacey, C., Mobasher, B., Panagia, N., & Rix, H. 2007, ApJ, 671, 1212

Oke, J. B. 1974, ApJS, 27, 21

Papovich, C., Finkelstein, S. L., Ferguson, H. C., Lotz, J. M., & Giavalisco, M. 2011, MNRAS, 412, 1123

Rauch, M., Haehnelt, M., Bunker, A., Becker, G., Marleau, F., Graham, J., Cristiani, S., Jarvis, M., Lacey, C., Morris, S., Peroux, C., Röttgering, H., & Theuns, T. 2008, ApJ, 681, 856

Ravindranath, S., Giavalisco, M., Ferguson, H. C., Conselice, C., Katz, N., Weinberg, M., Lotz, J., Dickinson, M., Fall, S. M., Mobasher, B., & Papovich, C. 2006, ApJ, 652, 963

Reddy, N. A., Steidel, C. C., Pettini, M., Adelberger, K. L., Shapley, A. E., Erb, D. K., & Dickinson, M. 2008, ApJS, 175, 48

Rodighiero, G., Daddi, E., Baronchelli, I., Cimatti, A., Renzini, A., Aussel, H., Popesso, P., Lutz, D., Andreani, P., Berta, S., Cava, A., Elbaz, D., Feltre, A., Fontana, A., Förster Schreiber, N. M., Franceschini, A., Genzel, R., Grazian, A., Gruppioni, C., Ilbert, O., Le Floch, E., Magdis, G., Magliocchetti, M., Magnelli, B., Maiolino, R., McCracken, H., Nordon, R., Poglitsch, A., Santini, P., Pozzi, F., Riguccini, L., Tacconi, L. J., Wuyts, S., & Zamorani, G. 2011, ApJ, 739, L40

Salimbeni, S., Fontana, A., Giallongo, E., Grazian, A., Menci, N., Pentericci, L., & Santini, P. 2009b, in American Institute of Physics Conference Series, Vol. 1111, American Institute of Physics Conference Series, ed. G. Giobbi, A. Tornambe, G. Raimondo, M. Limongi, L. A. Antonelli, N. Menci, & E. Brocato, 207–211

Salpeter, E. E. 1955, ApJ, 121, 161

Somerville, R. S., Barden, M., Rix, H.-W., Bell, E. F., Beckwith, S. V. W., Borch, A., Caldwell, J. A. R., Häußler, B., Heymans, C., Jahnke, K., Jogee, S., McIntosh, D. H., Meisenheimer, K., Peng, C. Y., Sánchez, S. F., Wisotzki, L., & Wolf, C. 2008, ApJ, 672, 776

Steidel, C. C., Erb, D. K., Shapley, A. E., Pettini, M., Reddy, N., Bogosavljević, M., Rudie, G. C., & Rakic, O. 2010, ApJ, 717, 289

Swinbank, A. M., Smail, I., Longmore, S., Harris, A. I., Baker, A. J., De Breuck, C., Richard, J., Edge, A. C., Ivison, R. J., Blundell, R., Coppin, K. E. K., Cox, P., Gurwell, M., Hainline, L. J., Krips, M., Lundgren, A., Neri, R., Siana, B., Siringo, G., Stark, D. P., Wilner, D., & Younger, J. D. 2010, Nature, 464, 733

Szomoru, D., Franx, M., Bouwens, R. J., van Dokkum, P. G., Labbé, I., Illingworth, G. D., & Trenti, M. 2011, ApJ, 735, L22+

Tacconi, L. J., Genzel, R., Neri, R., Cox, P., Cooper, M. C., Shapiro, K., Bolatto, A., Bouché, N., Bournaud, F., Burkert, A., Combes, F., Comerford, J., Davis, M., Schreiber, N. M. F., Garcia-Burillo, S., Gracia-Carpio, J., Lutz, D., Naab, T., Omont, A., Shapley, A., Sternberg, A., & Weiner, B. 2010, Nature, 463, 781

Tacconi, L. J., Genzel, R., Smail, I., Neri, R., Chapman, S. C., Ivison, R. J., Blain, A., Cox, P., Omont, A., Bertoldi, F., Greve, T., Förster Schreiber, N. M., Genel, S., Lutz, D., Swinbank, A. M., Shapley, A. E., Erb, D. K., Cimatti, A., Daddi, E., & Baker, A. J. 2008, ApJ, 680, 246

Trujillo, I., Conselice, C. J., Bundy, K., Cooper, M. C., Eisenhardt, P., & Ellis, R. S. 2007, MNRAS, 382, 109

Trujillo, I., Feulner, G., Goranova, Y., Hopp, U., Longhetti, M., Saracco, P., Bender, R., Braito, V., Della Ceca, R., Drory, N., Mannucci, F., & Severgnini, P. 2006, MNRAS, 373, L36

van Dokkum, P. G., Franx, M., Kriek, M., Holden, B., Illingworth, G. D., Magee, D., Bouwens, R., Marchesini, D., Quadri, R., Rudnick, G., Taylor, E. N., & Toft, S. 2008, ApJ, 677, L5

van Dokkum, P. G., Quadri, R., Marchesini, D., Rudnick, G., Franx, M., Gawiser, E., Herrera, D., Wuyts, S., Lira, P., Labbé, I., Maza, J., Illingworth, G. D., Förster Schreiber, N. M., Kriek, M., Rix, H.-W., Taylor, E. N., Toft, S., Webb, T., & Yi, S. K. 2006, ApJ, 638, L59

van Dokkum, P. G., Whitaker, K. E., Brammer, G., Franx, M., Kriek, M., Labbé, I., Marchesini, D., Quadri, R., Bezanson, R., Illingworth, G. D., Muzzin, A., Rudnick, G., Tal, T., & Wake, D. 2010, ApJ, 709, 1018

Wuyts, S., Forster Schreiber, N. M., Genzel, R., Guo, Y., Barro, G., Bell, E. F., Dekel, A., Faber, S. M., Ferguson, H. C., Giavalisco, M., Grogin, N. A., Hathi, N. P., Huang, K.-H., Kocevski, D. D., Koekemoer, A. M., Koo, D. C., Lotz, J., Lutz, D., McGrath, E., Newman, J. A., Rosario, D., Saintonge, A., Tacconi, L. J., Weiner, B. J., & van der Wel, A. 2012, ArXiv e-prints

Wuyts, S., Förster Schreiber, N. M., van der Wel, A., Magnelli, B., Guo, Y., Genzel, R., Lutz, D., Aussel, H., Barro, G., Berta, S., Cava, A., Graciá-Carpio, J., Hathi, N. P., Huang, K.-H., Kocevski, D. D., Koekemoer, A. M., Lee, K.-S., Le Floc'h, E., McGrath, E. J., Nordon, R., Popesso, P., Pozzi, F., Riguccini, L., Rodighiero, G., Saintonge, A., & Tacconi, L. 2011, ApJ, 742, 96

Table 1: Properties of Star-forming Galaxies at z∼2

ID	RA	DEC	z	M_{star}	SFR	E(B-V)	U-V	M_V
	J2000	J2000		Log(M*/$M_\odot$)	$M_\odot$/yr			
20565	53.1422430	-27.7954120	2.016	10.28± 0.05	30.45± 6.09	0.20±0.05	0.64±0.00	-21.50± 0.00
21739	53.1485260	-27.7969040	1.765	9.92± 0.02	33.64± 6.73	0.10±0.05	0.23±0.00	-21.54± 0.00
21852	53.1492150	-27.7788090	1.850	10.35± 0.04	40.35± 8.07	0.25±0.05	0.61±0.00	-21.42± 0.00
22284	53.1516190	-27.7964320	1.767	10.51± 0.12	51.32± 10.26	0.15±0.05	0.48±0.00	-22.15± 0.00
23013	53.1556430	-27.7792950	1.846	10.73± 0.10	162.39± 32.48	0.30±0.05	0.62±0.00	-22.51± 0.00
24033	53.1616630	-27.7874320	1.836	10.79± 0.15	111.00± 31.07	0.35±0.06	0.77±0.00	-22.10± 0.00
24684	53.1655460	-27.7697760	1.552	11.06± 0.07	10.93± 6.60	0.20±0.13	1.36±0.00	-21.92± 0.00
24919	53.1668940	-27.7987410	1.998	11.02± 0.02	423.67± 84.73	0.40±0.05	0.74±0.00	-23.03± 0.00
26067	53.1743180	-27.7825190	1.994	10.61± 0.11	64.39± 12.88	0.25±0.05	0.67±0.00	-21.97± 0.00
27101	53.1817060	-27.7830010	1.570	10.21± 0.05	64.68± 17.49	0.30±0.05	0.69±0.00	-21.46± 0.00

Table 2:: Properties of Clumps and "Disks"

ID 1	**ID 2** [1]	**d**	$\mathbf{M_{star}}$ [2]	**SFR**	**E(B-V)**	**age**	**U-V**	$\mathbf{M_V}$
Galaxy	**Clump**	$\frac{d_{proj}}{r_{kron}}$	$\log(M_\odot)$	$M_\odot yr^{-1}$		**Gyr**		
20565	1	0.24	8.80± 0.00	3.77± 0.75	0.25±0.05	0.20±0.00	0.35±0.17	-18.30± 0.14
			8.88± 0.04	4.45± 0.89	0.25±0.05	0.20±0.02	0.40±0.14	-18.52± 0.12
			8.77± 0.00	3.49± 0.70	0.25±0.05	0.20±0.00	0.32±0.15	-18.20± 0.13
20565	2	0.01	9.27± 0.05	7.52± 2.04	0.30±0.05	0.30±0.04	0.69±0.14	-19.15± 0.12
			9.42± 0.03	5.40± 2.01	0.25±0.05	0.60±0.05	0.68±0.13	-19.25± 0.10
			9.15± 0.02	5.62± 1.23	0.30±0.05	0.30±0.02	0.67±0.19	-18.80± 0.15
20565	3	0.16	9.05± 0.06	6.72± 2.23	0.30±0.05	0.20±0.03	0.61±0.15	-18.77± 0.12
			9.11± 0.06	7.66± 2.55	0.30±0.05	0.20±0.03	0.62±0.14	-18.92± 0.12
			9.08± 0.09	48.18± 26.62	0.30±0.05	0.40±0.13	0.54±0.20	-18.62± 0.18
20565	D	—-	10.24± 0.03	24.62± 4.92	0.20±0.05	0.90±0.07	0.66±0.00	-21.20± 0.00
			10.28± 0.05	30.45± 6.09	0.20±0.05	0.60±0.06	0.64±0.00	-21.50± 0.00
			10.31± 0.05	32.69± 6.54	0.20±0.05	0.60±0.06	0.65±0.00	-21.59± 0.00
21739	1	0.25	8.97± 0.04	5.52± 1.10	0.20±0.05	0.20±0.02	0.40±0.11	-18.98± 0.08
			9.03± 0.03	6.37± 1.42	0.20±0.05	0.20±0.02	0.38±0.10	-19.11± 0.07
			8.86± 0.04	4.33± 0.87	0.20±0.05	0.20±0.02	0.41±0.12	-18.71± 0.10
21739	2	0.22	8.16± 0.00	14.84± 2.97	0.25±0.05	0.01±0.00	0.12±0.11	-18.52± 0.07
			8.23± 0.00	17.36± 3.47	0.25±0.05	0.01±0.00	0.14±0.09	-18.71± 0.07
			8.12± 0.00	13.47± 2.69	0.25±0.05	0.01±0.00	0.03±0.12	-18.35± 0.10
21739	3	0.07	7.97± 0.29	9.51± 2.38	0.20±0.06	0.01±0.01	-0.04±0.13	-18.24± 0.10
			8.65± 0.07	1.77± 0.45	0.05±0.05	0.30±0.08	0.01±0.10	-18.49± 0.08
			7.87± 0.00	7.53± 1.51	0.20±0.05	0.01±0.00	-0.08±0.18	-17.95± 0.14
21739	4	0.34	8.09± 0.02	0.50± 0.10	0.05±0.05	0.30±0.03	0.15±0.17	-17.18± 0.10
			8.27± 0.07	0.61± 0.12	0.00±0.05	0.20±0.03	0.19±0.09	-17.73± 0.07
			8.30± 0.05	0.49± 0.10	0.05±0.05	0.50±0.06	0.24±0.14	-17.31± 0.10
21739	5	0.52	7.74± 0.10	0.70± 0.51	0.05±0.05	0.09±0.03	0.13±0.18	-17.04± 0.13

Table 2 – continued

ID 1	ID 2	d	M_{star}	SFR	E(B-V)	age	U-V	M_V
Galaxy	Clump	$\frac{d_{proj}}{r_{kron}}$	$\log(M_\odot)$	$M_\odot yr^{-1}$		Gyr		
			8.19± 0.01	0.92± 0.18	0.05±0.05	0.20±0.00	0.18±0.11	-17.65± 0.09
			8.00± 0.01	0.60± 0.12	0.05±0.05	0.20±0.00	0.20±0.15	-17.18± 0.12
21739	D	—-	9.80± 0.04	25.18± 5.04	0.10±0.05	0.30±0.05	0.25±0.00	-21.24± 0.00
			9.92± 0.02	33.64± 6.73	0.10±0.05	0.30±0.03	0.23±0.00	-21.54± 0.00
			9.96± 0.02	36.81± 7.36	0.10±0.05	0.30±0.03	0.24±0.00	-21.64± 0.00
21852	1	0.37	8.84± 0.07	2.09± 0.42	0.25±0.05	0.40±0.07	0.52±0.15	-17.97± 0.12
			8.93± 0.08	2.61± 0.52	0.25±0.05	0.40±0.07	0.54±0.12	-18.24± 0.08
			8.82± 0.03	1.17± 0.57	0.20±0.05	0.70±0.03	0.60±0.17	-17.78± 0.14
21852	2	0.10	9.01± 0.08	3.37± 0.67	0.25±0.05	0.20±0.03	0.67±0.13	-18.58± 0.09
			9.13± 0.10	3.09± 0.62	0.25±0.05	0.30±0.07	0.66±0.14	-18.74± 0.10
			9.05± 0.03	2.75± 0.55	0.30±0.05	0.50±0.03	0.68±0.22	-18.15± 0.15
21852	3	0.20	8.83± 0.03	2.69± 0.77	0.25±0.05	0.30±0.02	0.51±0.18	-18.17± 0.12
			9.00± 0.04	2.07± 0.41	0.20±0.05	0.60±0.09	0.53±0.16	-18.40± 0.10
			8.54± 0.03	2.07± 0.41	0.25±0.05	0.20±0.02	0.46±0.29	-17.68± 0.22
21852	4	0.09	9.34± 0.03	6.67± 1.33	0.40±0.05	0.40±0.03	0.80±0.14	-18.62± 0.09
			9.40± 0.03	5.22± 1.04	0.35±0.05	0.60±0.06	0.77±0.14	-18.78± 0.09
			9.27± 0.04	10.98± 2.20	0.65±0.05	0.20±0.02	1.05±0.37	-17.80± 0.25
21852	D	—-	9.99± 0.15	10.83± 2.91	0.15±0.06	0.30±0.07	0.60±0.00	-21.12± 0.00
			10.35± 0.04	40.35± 8.07	0.25±0.05	0.70±0.07	0.61±0.00	-21.42± 0.00
			10.41± 0.03	46.11± 9.22	0.25±0.05	0.70±0.06	0.61±0.00	-21.55± 0.00
22284	1	0.24	8.86± 0.06	2.92± 1.79	0.10±0.05	0.30±0.05	0.26±0.14	-18.91± 0.10
			8.96± 0.03	5.47± 1.22	0.15±0.05	0.20±0.02	0.30±0.10	-19.16± 0.08
			8.72± 0.04	2.08± 0.42	0.10±0.05	0.30±0.05	0.33±0.19	-18.57± 0.14
22284	2	0.11	9.47± 0.11	3.76± 0.75	0.25±0.05	0.40±0.09	0.84±0.14	-19.28± 0.10
			9.42± 0.18	2.91± 0.58	0.20±0.05	0.30±0.11	0.78±0.10	-19.47± 0.08
			9.38± 0.12	1.89± 0.38	0.25±0.05	0.60±0.13	0.92±0.17	-18.84± 0.13
22284	3	0.39	7.70± 0.00	5.11± 1.02	0.20±0.05	0.01±0.00	-0.16±0.20	-17.43± 0.15
			8.43± 0.07	3.07± 0.62	0.15±0.05	0.10±0.02	0.12±0.12	-18.21± 0.08
			7.61± 0.00	4.13± 0.83	0.20±0.05	0.01±0.00	0.00±0.26	-17.32± 0.20
22284	D	—-	10.42± 0.01	64.88± 12.98	0.20±0.05	0.50±0.02	0.48±0.00	-21.99± 0.00
			10.51± 0.12	51.32± 10.26	0.15±0.05	0.80±0.21	0.48±0.00	-22.15± 0.00
			10.36± 0.11	51.99± 10.40	0.15±0.05	0.30±0.07	0.48±0.00	-22.23± 0.00
23013	1	0.04	10.03± 0.01	63.07± 12.61	0.55±0.05	0.20±0.00	0.84±0.12	-20.07± 0.09
			10.08± 0.04	48.06± 9.61	0.50±0.05	0.30±0.03	0.81±0.11	-20.19± 0.07
			9.89± 0.04	30.98± 6.20	0.50±0.05	0.30±0.05	0.84±0.16	-19.76± 0.11
23013	2	0.35	9.01± 0.07	11.72± 2.38	0.30±0.05	0.10±0.02	0.42±0.15	-18.97± 0.10
			9.25± 0.05	17.40± 3.70	0.30±0.05	0.20±0.05	0.46±0.11	-19.28± 0.09
			8.80± 0.02	9.06± 1.81	0.30±0.05	0.08±0.00	0.39±0.18	-18.65± 0.14
23013	3	0.19	9.29± 0.01	22.52± 4.50	0.45±0.05	0.10±0.00	0.66±0.17	-19.11± 0.11

Table 2 – continued

ID 1	ID 2	d	M_{star}	SFR	E(B-V)	age	U-V	M_V
Galaxy	Clump	$\frac{d_{proj}}{r_{kron}}$	$\log(M_\odot)$	$M_\odot yr^{-1}$		Gyr		
			9.49± 0.01	18.45± 3.69	0.40±0.05	0.20±0.00	0.65±0.13	-19.39± 0.10
			9.12± 0.06	16.62± 7.61	0.45±0.05	0.09±0.02	0.63±0.24	-18.71± 0.17
23013	4	0.65	7.02± 0.00	1.06± 0.21	0.00±0.05	0.01±0.00	-0.71±0.31	-16.34± 0.29
			8.25± 0.18	2.04± 8.36	0.10±0.05	0.10±0.07	0.17±0.10	-18.03± 0.06
			8.03± 0.02	1.74± 0.35	0.10±0.05	0.07±0.00	0.11±0.13	-17.67± 0.09
23013	D	—-	10.63± 0.10	131.35± 26.27	0.30±0.05	0.40±0.08	0.61±0.00	-22.29± 0.00
			10.73± 0.10	162.39± 32.48	0.30±0.05	0.40±0.08	0.62±0.00	-22.51± 0.00
			10.76± 0.03	176.46± 35.29	0.30±0.05	0.40±0.02	0.62±0.00	-22.61± 0.00
24033	1	0.30	9.09± 0.04	49.43± 31.14	0.25±0.05	0.40±0.03	0.50±0.14	-18.88± 0.11
			9.27± 0.10	54.11± 27.27	0.25±0.05	0.60±0.17	0.54±0.12	-19.10± 0.09
			8.87± 0.04	14.83± 5.16	0.25±0.05	0.20±0.02	0.43±0.16	-18.65± 0.12
24033	2	0.12	9.50± 0.10	9.66± 3.97	0.35±0.05	0.40±0.11	0.75±0.16	-19.22± 0.10
			9.56± 0.15	11.05± 7.42	0.35±0.05	0.40±0.16	0.75±0.15	-19.38± 0.09
			9.20± 0.03	6.37± 1.27	0.35±0.05	0.30±0.02	0.71±0.21	-18.72± 0.17
24033	3	0.07	10.23± 0.09	41.96± 8.39	0.65±0.05	0.50±0.06	1.19±0.14	-19.63± 0.09
			10.26± 0.09	25.24± 5.05	0.55±0.05	0.90±0.18	1.14±0.11	-19.75± 0.08
			10.11± 0.10	14.20± 5.08	0.70±0.09	0.30±0.02	1.45±0.26	-19.07± 0.15
24033	4	0.27	9.45± 0.04	11.23± 2.25	0.50±0.05	0.30±0.03	0.70±0.17	-18.58± 0.11
			9.55± 0.08	10.77± 2.15	0.45±0.05	0.40±0.07	0.71±0.14	-18.86± 0.09
			9.20± 0.00	9.48± 1.90	0.50±0.05	0.20±0.00	0.73±0.23	-18.23± 0.15
24033	D	—-	10.70± 0.16	78.01± 20.17	0.35±0.06	0.80±0.20	0.75±0.00	-21.76± 0.00
			10.79± 0.15	111.00± 31.07	0.35±0.06	0.70±0.16	0.77±0.00	-22.10± 0.00
			10.85± 0.15	125.39± 33.86	0.35±0.06	0.70±0.16	0.78±0.00	-22.23± 0.00
24684	1	0.20	8.86± 0.14	2.88± 3.10	0.35±0.05	0.30±0.12	0.74±0.12	-17.85± 0.09
			9.20± 0.13	3.30± 3.30	0.35±0.05	0.60±0.24	0.92±0.10	-18.33± 0.07
			8.70± 0.06	2.94± 0.59	0.35±0.05	0.20±0.03	0.63±0.16	-17.61± 0.12
24684	2	0.04	10.48± 0.31	0.00± 0.00	0.30±0.40	3.00±0.00	2.47±0.13	-19.38± 0.06
			10.87± 0.12	3.27± 2.42	0.60±0.20	3.00±0.00	2.26±0.10	-19.51± 0.07
			10.93± 0.01	3.78± 2.33	0.75±0.14	3.00±0.00	2.60±0.16	-19.10± 0.07
24684	3	0.32	7.75± 0.03	0.91± 0.18	0.10±0.05	0.07±0.01	0.03±0.18	-16.91± 0.15
			8.76± 0.04	0.53± 0.11	0.05±0.05	1.40±0.19	0.63±0.08	-17.87± 0.06
			8.05± 0.04	0.45± 0.09	0.05±0.05	0.30±0.02	0.37±0.17	-17.21± 0.12
24684	4	0.13	9.37± 0.07	1.69± 0.38	0.40±0.05	1.80±0.23	1.22±0.17	-17.83± 0.11
			9.74± 0.01	2.43± 0.49	0.40±0.05	3.00±0.05	1.27±0.10	-18.31± 0.08
			9.37± 0.01	1.19± 0.24	0.35±0.05	2.60±0.09	1.17±0.19	-17.74± 0.13
24684	5	0.31	8.63± 0.02	1.70± 0.34	0.35±0.05	0.30±0.03	0.71±0.18	-17.28± 0.13
			9.20± 0.04	2.23± 0.61	0.35±0.05	0.90±0.09	0.97±0.11	-18.00± 0.06
			8.72± 0.04	0.94± 0.49	0.30±0.05	0.70±0.14	0.83±0.24	-17.15± 0.15
24684	D	—-	11.01± 0.09	12.58± 5.73	0.25±0.12	2.20±0.17	1.36±0.01	-21.71± 0.00

Table 2 – continued

ID 1	ID 2	d	M_{star}	SFR	E(B-V)	age	U-V	M_V
Galaxy	Clump	$\frac{d_{proj}}{r_{kron}}$	$\log(M_\odot)$	$M_\odot yr^{-1}$		Gyr		
			11.06± 0.07	10.93± 6.60	0.20±0.13	2.40±0.13	1.36±0.00	-21.92± 0.00
			11.10± 0.09	11.86± 6.59	0.20±0.13	2.40±0.13	1.37±0.00	-22.01± 0.00
24919	1	0.22	9.23± 0.01	21.62± 4.32	0.30±0.05	0.09±0.00	0.30±0.18	-19.60± 0.12
			9.30± 0.10	37.34± 7.47	0.35±0.05	0.06±0.02	0.39±0.15	-19.88± 0.12
			9.21± 0.00	18.85± 3.77	0.30±0.05	0.10±0.00	0.35±0.19	-19.50± 0.16
24919	2	0.07	9.99± 0.03	29.81± 5.96	0.40±0.05	0.40±0.03	0.93±0.15	-20.26± 0.12
			10.06± 0.03	35.04± 7.01	0.40±0.05	0.40±0.03	0.90±0.12	-20.42± 0.10
			9.76± 0.00	23.24± 4.65	0.40±0.05	0.30±0.00	0.91±0.20	-19.92± 0.16
24919	3	0.25	9.30± 0.08	37.13± 7.43	0.55±0.05	0.06±0.02	0.76±0.18	-19.03± 0.15
			9.60± 0.04	23.63± 4.73	0.45±0.05	0.20±0.02	0.75±0.13	-19.47± 0.11
			9.26± 0.02	25.65± 5.13	0.50±0.05	0.08±0.00	0.70±0.23	-18.91± 0.17
24919	4	0.25	9.69± 0.00	494.21± 98.84	0.95±0.05	0.01±0.00	1.07±0.16	-19.26± 0.14
			10.02± 0.02	42.12± 8.42	0.60±0.05	0.30±0.03	0.97±0.13	-19.63± 0.09
			9.72± 0.00	530.72±106.14	1.00±0.05	0.01±0.00	1.04±0.23	-19.06± 0.19
24919	5	0.33	9.27± 0.04	7.46± 1.49	0.35±0.05	0.30±0.03	0.56±0.20	-18.76± 0.17
			9.45± 0.04	11.22± 2.24	0.35±0.05	0.30±0.05	0.63±0.14	-19.30± 0.12
			9.09± 0.00	7.22± 1.44	0.35±0.05	0.20±0.00	0.60±0.30	-18.57± 0.25
24919	D	—-	10.92± 0.05	334.27± 66.85	0.40±0.05	0.30±0.05	0.74±0.00	-22.80± 0.00
			11.02± 0.02	423.67± 84.73	0.40±0.05	0.30±0.03	0.74±0.00	-23.03± 0.00
			11.06± 0.03	463.33± 92.67	0.40±0.05	0.30±0.02	0.74±0.00	-23.13± 0.00
26067	1	0.09	9.35± 0.07	23.57± 7.39	0.20±0.05	0.60±0.10	0.55±0.14	-19.44± 0.11
			9.36± 0.04	9.27± 1.85	0.20±0.05	0.40±0.03	0.56±0.14	-19.57± 0.10
			9.14± 0.02	5.56± 1.21	0.20±0.05	0.30±0.02	0.52±0.15	-19.18± 0.15
26067	2	0.13	9.87± 0.06	13.36± 2.67	0.40±0.05	0.70±0.10	0.83±0.12	-19.53± 0.09
			9.93± 0.08	10.71± 2.14	0.35±0.05	1.00±0.20	0.81±0.12	-19.65± 0.10
			9.77± 0.06	10.50± 2.10	0.40±0.05	0.70±0.10	0.85±0.20	-19.28± 0.15
26067	D	—-	10.55± 0.05	49.82± 9.96	0.25±0.05	0.90±0.09	0.66±0.00	-21.72± 0.00
			10.61± 0.11	64.39± 12.88	0.25±0.05	0.80±0.20	0.67±0.00	-21.97± 0.00
			10.64± 0.11	68.62± 13.72	0.25±0.05	0.80±0.20	0.67±0.00	-22.04± 0.00
27101	1	0.06	9.61± 0.05	2.91± 0.58	0.30±0.05	1.80±0.20	1.02±0.10	-18.81± 0.07
			9.63± 0.04	3.91± 0.78	0.30±0.05	1.40±0.16	0.98±0.10	-18.95± 0.06
			9.39± 0.07	2.58± 2.85	0.30±0.05	1.20±0.28	0.99±0.14	-18.55± 0.10
27101	2	0.17	8.52± 0.01	5.32± 1.06	0.30±0.05	0.07±0.00	0.50±0.13	-18.08± 0.09
			8.71± 0.64	5.89± 44.74	0.30±0.05	0.10±0.09	0.54±0.09	-18.35± 0.06
			8.58± 0.02	4.32± 0.86	0.30±0.05	0.10±0.01	0.55±0.14	-18.01± 0.10
27101	3	0.17	8.06± 0.00	11.78± 2.36	0.40±0.05	0.01±0.00	0.10±0.12	-17.45± 0.09
			8.18± 0.00	15.62± 3.12	0.40±0.05	0.01±0.00	0.26±0.09	-17.89± 0.06
			7.98± 0.00	9.83± 1.97	0.40±0.05	0.01±0.00	0.10±0.17	-17.25± 0.13
27101	4	0.17	9.00± 0.07	0.82± 0.21	0.20±0.05	1.60±0.28	0.81±0.16	-17.83± 0.10

Table 2 – continued

ID 1	**ID 2**	**d**	$\mathbf{M_{star}}$	**SFR**	**E(B-V)**	**age**	**U-V**	$\mathbf{M_V}$
Galaxy	**Clump**	$\frac{\mathbf{d_{proj}}}{\mathbf{r_{kron}}}$	$\mathbf{log(M_\odot)}$	$\mathbf{M_\odot yr^{-1}}$		**Gyr**		
			9.14± 0.04	1.26± 1.11	0.20±0.05	1.40±0.27	0.78±0.08	-18.16± 0.06
			8.77± 0.16	1.21± 1.16	0.25±0.05	0.60±0.31	0.77±0.17	-17.68± 0.13
27101	5	0.27	8.59± 0.07	0.41± 0.46	0.10±0.05	1.20±0.28	0.61±0.15	-17.36± 0.10
			8.80± 0.06	0.89± 0.18	0.15±0.05	0.90±0.12	0.64±0.10	-17.82± 0.07
			8.16± 0.16	0.58± 1.30	0.15±0.05	0.30±0.18	0.45±0.21	-16.95± 0.15
27101	D	—-	10.10± 0.06	50.42± 15.87	0.30±0.05	0.30±0.05	0.70±0.01	-21.19± 0.00
			10.21± 0.05	64.68± 17.49	0.30±0.05	0.30±0.04	0.69±0.00	-21.46± 0.00
			10.25± 0.03	70.69± 14.14	0.30±0.05	0.30±0.02	0.70±0.00	-21.56± 0.00

Table 3: Comparison o9 Derived Properties of Three Galaxies in Our Sample and Elmegreen & Elmegreen (2005)

Galaxy	ID	z	N_{clump}	Age_{clump} (Gyr)	Age_{disk} (Gyr)	$< M_{clump} > 10^9 M_\odot$	f_{mass}	$M_{gal} 10^{10} M_\odot$	$< SFR_{clump} > M_\odot yr^{-1}$
1	21739	1.765	5	0.12	0.30	0.27	0.16	0.8	6.2
	3465+	2.4	11	0.22	1.80	0.87	0.28	3.5	4.5
2	22284	1.767	3	0.24	0.50	1.25	0.12	3.2	3.9
	3483	2.2	12	0.26	2.02	1.31	0.32	4.9	1.0
3	27101	1.570	5	0.94	0.30	1.18	0.36	1.6	4.3
	6462+	2.8	8	0.31	2.82	1.57	0.22	5.7	0.9

Note: For each galaxy, the first line shows the data in our work, while the second line shows the data in Elmegreen et al. (2005). In this table, we have applied the relations in Sec. 6.1 to convert the Chabrier IMF to the Salpeter IMF.

[1]Numbers stand for ID of clumps in the z-band images of Figure 1, while "D" stands for the diffuse "disk" component.

[2]For each clump, properties derived under different background subtraction schemes are listed: global constant background (1st line), zero background (2nd line) and local background (3rd line).